

# Data assimilation using the particle filter for identifying the elasto-plastic material properties of geomaterials

Akira Murakami<sup>1,\*†</sup>, Takayuki Shuku<sup>2</sup>, Shin-ichi Nishimura<sup>2</sup>, Kazunori Fujisawa<sup>2</sup> and Kazuyuki Nakamura<sup>3</sup>

<sup>1</sup>*Graduate School of Agriculture, Kyoto University, Sakyo-ku, Kyoto, Japan*

<sup>2</sup>*Graduate School of Environmental and Life Science, Okayama University, Kita-ku, Okayama, Japan*

<sup>3</sup>*Graduate School of Advanced Mathematical Sciences, Meiji University, Tama-ku, Kawasaki, Japan*

## SUMMARY

A computational method, incorporating the finite element model (FEM) into data assimilation using the particle filter, is presented for identifying elasto-plastic material properties based on sequential measurements under the known changing traction boundary conditions to overcome some difficulties in identifying the parameters for elasto-plastic problems from which the existing inverse analysis strategies have suffered. A soil–water coupled problem, which uses the elasto-plastic constitutive model, is dealt with as the geotechnical application. Measured data on the settlement and the pore pressure are obtained from a synthetic FEM computation as the forward problem under the known parameters to be identified for both the element tests and the ground behavior during the embankment construction sequence. Parameter identification for elasto-plastic problems, such as soil behavior, should be made by considering the measurements of deformation and/or pore pressure step by step from the initial stage of construction and throughout the deformation history under the changing traction boundary conditions because of the embankment or the excavation because the ground behavior is highly dependent on the loading history. Thus, it appears that sequential data assimilation techniques, such as the particle filter, are the preferable tools that can provide estimates of the state variables, that is, deformation, pore pressure, and unknown parameters, for the constitutive model in geotechnical practice. The present paper discusses the priority of the particle filter in its application to initial/boundary value problems for elasto-plastic materials and demonstrates a couple of numerical examples. Copyright © 2012 John Wiley & Sons, Ltd.

Received 6 November 2010; Revised 16 April 2012; Accepted 9 June 2012

KEY WORDS: data assimilation; particle filter; inverse problem; soil-water coupled FEM

## 1. INTRODUCTION

It is common practice in geotechnical engineering to utilize numerical simulations based on the soil–water coupled finite element model (FEM) with a sophisticated constitutive model for elasto-plastic materials to obtain prior predictions of the behavior of soil structures and their foundations at the design stage. During the construction stage, on the other hand, observational programs are set up to evaluate the design assumptions and the current construction conditions under such numerical predictions for accuracy in future performances.

However, discrepancies are often found between the numerical predictions and the corresponding field measurements in terms of deformation and pore pressure. This is due to the uncertainty of the initial and the boundary conditions of the governing partial differential equation and/or the

\*Correspondence to: Akira Murakami, Graduate School of Agriculture, Kyoto University, Kitashirakawa-oiwakecho, Sakyo-ku, 606-8502, Kyoto, Japan.

†E-mail: murakami.akira.5u@kyoto-u.ac.jp

parameters of the elasto-plastic constitutive model, which should be assessed from site investigations and based on the results of laboratory tests conducted prior to construction. Inverse analyses have been applied to performance observations in engineering practice to modify such uncertain conditions and parameters for bridging the gap between observations and predictions [1, 2] and for giving feedback regarding the re-evaluation of the numerical simulations for subsequent construction sequences as a quantifiable observational method. Several numerical strategies for inverse problems have been proposed in various fields of engineering over the last few decades, and some have been applied to geotechnical problems, as described in Refs. [3–8] and recently in Refs. [9–12], and references therein.

The present paper focuses on the identification of the initial conditions and the parameters within the elasto-plastic constitutive model based on field measurements for geotechnical applications. Inverse problems in linear elasticity have been successfully solved by both analytical and numerical means. On the other hand, there still remain some difficulties in identifying the elasto-plastic parameters [13] because for elasto-plastic material, the current deformation does not have one-to-one correspondence with the stress state at the same moment but depends on the loading path from the initial stage to the current stage. Then, the observation of the deformation, along with full knowledge of the loading history, is necessary for the parameter identification of the elasto-plastic constitutive model. Related literature has tried to identify the parameters, such as Young's modulus, the friction angle, the coefficient of earth pressure at rest, poroelastic parameters and so on, based on the minimization of the objective function, by means of the gradient method, GA and a sensitivity analysis. However, none of them considered the deformation associated with the loading history from the initial stage up to the current stage for the identification of the plastic parameters. Sequential data assimilation techniques, such as the PF, are applicable to this type of inverse problem because the time evolution of state variables, that is, displacement and pore pressure for geotechnics, under the controlled input, like the external loading, is incorporated into the system equation in a rational manner without any limitations. The PF can easily deal with nonlinear state equations and is robust when employing the Monte Carlo method in conjunction with a numerical simulation, for example, the soil–water-coupled finite element analysis with the elasto-plastic model. Saturated soil is treated as an elasto-plastic material and its behavior relies on the parameters of an elasto-plastic constitutive model, the initial stress, and the stress paths up to the current stress state, because of the different patterns of loading history, whereas the deformation of an elastic material is independent of such factors. From the viewpoint of an inverse analysis, the unknown parameters of an elasto-plastic material can hardly be identified without knowledge of the loading history, whereas those of an elastic material can be identified by the deformation and the stress state at the current stage.

Let us show an example [14]. Consider the synthetic behavior of a saturated soil deposit through a soil–water coupled FEM model, which follows an elasto-plastic constitutive equation under different embankment and excavation loading histories, as seen in Figure 1. Four different loading and excavation histories are listed under the material parameters, and a different set of initial stress parameters, for example,  $\sigma'_{v0}$  and  $K_0$ , are adopted, as given in Table I. Figure 2 reveals that the artificial settlements at the black circles, beneath the hypothetical embankment loading obtained from the FEM computation, are dependent on either the different sequences of external action or a different set of elasto-plastic and initial stress parameters listed in Table II. Then, the inverse problem concerning the determination of the parameters for the elasto-plastic constitutive model becomes ill posed in the uniqueness of the solutions based on the settlement of the soil deposit unless we have knowledge of the embankment loading history. This is because we cannot discriminate between two settlement curves under different loading histories from those because of different parameters, even if the final shapes of the soil structure are the same.

To tackle the above-mentioned difficulty, a so-called 'data assimilation' (DA) is advantageous for solving this type of inverse problem by conducting step-by-step observations and procuring full knowledge of the loading history. DA is a concept used in geophysics that combines observations with numerical models; it is one of the alternative remedies for improving predictions by adjusting uncertain initial conditions and/or parameters by taking observations into consideration. There are two types of DA strategies, the batch-type DA, for example, 4DVAR [15] and the sequential DA, for example, the ensemble Kalman filter (EnKF) [16, 17] and the particle filter (PF) [18, 19]. The

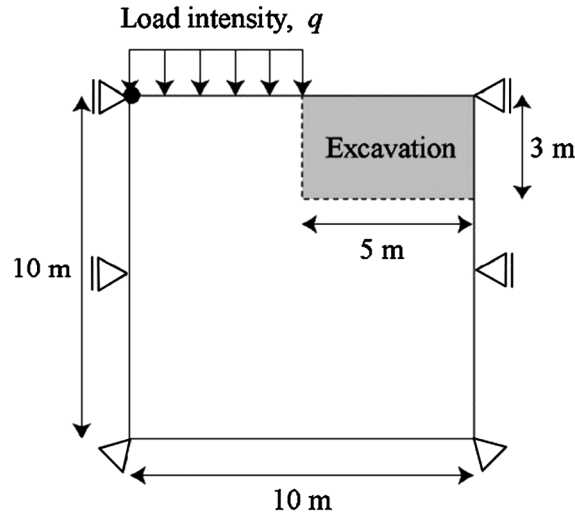


Figure 1. Hypothetical problem.

Table I. Material parameters for elasto-plastic analysis.

$\Lambda = 1 - \kappa/\lambda = 0.57$ ,  $D = 0.53$ ,  $M = 1.0$ ,  $\nu = 0.33$ ,  $K_0 = 0.5$ ,  $\text{OCR} = 1$ ,  
 $k = 1.0 \times 10^{-5}$  (cm/sec),  $\sigma'_{v0} = 100\text{kPa}$

where  $\Lambda$  is the irreversible ratio,  $\lambda$  is the compression index,  $\kappa$  is the swelling index,  $D$  is the dilatancy coefficient,  $M$  is the stress ratio at the critical state,  $\nu$  is Poisson's ratio,  $K_0$  is the coefficient of earth pressure at rest,  $\text{OCR}$  is the overconsolidation ratio,  $k$  is the permeability, and  $\sigma'_{v0}$  is the initial vertical effective stress.

Table II. Different loading histories related to construction sequences.

Cases	Construction sequences
#1	1) Embankment loading for 10 days at a rate of 5.88 kN/day; 2) Excavation for 9 days; 3) No external action
#2	1) Embankment loading for 1000 days at a rate of 0.0588 kN/day; 2) Excavation for 9 days; 3) No external action
#3	1) Excavation for 9 days; 2) Embankment loading for 10 days at a rate of 5.88 kN/day; 3) No external action
#4	1) Excavation for 9 days; 2) Embankment loading for 1000 days at a rate of 0.0588 kN/day; 3) No external action
#1'	Same sequence as Case 1, except for a value of 150 kPa for $\sigma'_{v0}$
#1''	Same sequence as Case 1, except for a value of 0.6 for $K_0$

All the excavation work was done at a rate of 0.33 m/day.

EnKF and the PF have been developed for strongly nonlinear problems as alternative data assimilation strategies to the traditional Kalman filter [20], the extended Kalman filter, and the unscented Kalman filter, which have been applied to inverse problems in geomechanics [21, 22] and in structural elasto-plasticity [23, 24]. In the earliest studies, several attempts were made to adopt the EnKF and the PF for data assimilation in civil engineering applications, for example, DA for transient flows in geologic formations [25] and the identification of elastic constants in foundations under embankment loading [26] by the EnKF, and a nonlinear structural dynamical system identification by the unscented Kalman filter [27] and the PF [28–30]. Herein, the focus is placed on the sequential DA, in particular, the PF.

The PF is one of the Monte Carlo nonlinear filtering methods to maximize the Bayesian likelihood and to provide the 'sequential Bayesian estimation' where noise in the PF does not correspond to a measurement error but to the gap between the numerical simulation and the observation. This means that the probability function of the parameters is approximated by samples and updated by Bayes' rule with each observation, and as a consequence, we can obtain the prediction of the deformation, which reflects all observations up to that time based on the time update scheme compared with an ordinary Bayesian or a likelihood approach. The application of the PF reduces the noise in the above sense and leads to a better prediction.

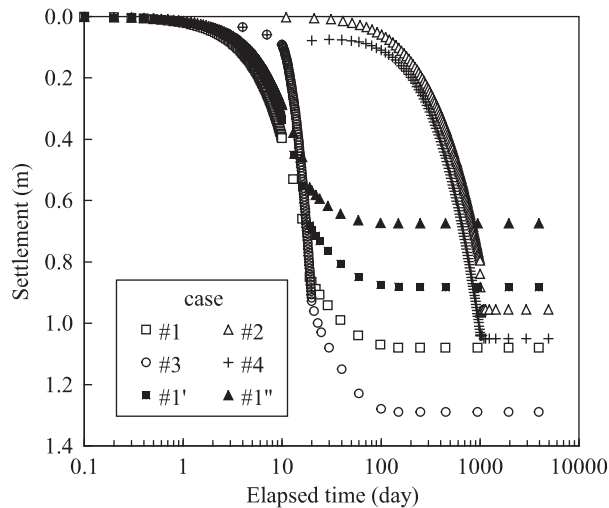


Figure 2. Settlement under different loading histories or parameters.

The PF is not an optimization tool or algorithm, like genetic algorithms and conjugated gradient methods, but estimates the probability density function of parameter sets without objective functions. The relationship between observations and direct calculations is given by the likelihood function derived from the observation equation. That is, the PF can give not only the best parameter value but also the realization probability of other parameter values, such as the second best and the just-off best values for parameters. The PF does not need offline training as in artificial neural networks. Instead of the repetition of training, the PF employs parallel numerical simulations called ‘particles’ that can be regarded as independent scenarios. The preciseness of the estimation and the prediction is improved by increasing the number of particles. Also, the more observation data we obtain, the more appropriate values for the parameters, which closely simulate the observation, can be identified.

The purpose of this paper is to describe the priority of the PF in its application to initial and boundary value problems for elasto-plastic materials and to demonstrate a couple of numerical examples for both hypothetical and actual soil tests. If we adopt the initial stress parameters, which affect the initial shape of the yield function in the stress space and are not easy to determine a priori for practical problems, or the parameters of the elasto-plastic constitutive model, such as  $\lambda$  and  $\kappa$ , as the unknowns to be identified, an alternative inverse analysis should be made by tracking the loading history along the boundary. To accomplish this purpose, synthetic settlement observations generated by the FEM simulation, based on the known elasto-plastic parameters, are analyzed to examine the applicability of the proposed computational procedure. Hypothetical element tests and the ground behavior under continuous embankment loading for a soft soil foundation are dealt with to verify the applicability of the proposed procedure.

The rest of the paper is arranged as follows. Section 2 presents a brief description of the Cam-clay mode for finite strain. Section 3 provides the computational procedure of the PF for geotechnical applications. Numerical examples are presented in Section 4 for both hypothetical element tests and ground behavior under continuous embankment loading to demonstrate the performance of the PF in conjunction with the soil–water coupled FEM. Conclusions will follow in the last section.

## 2. CONSTITUTIVE MODEL FOR SOIL

### 2.1. Constitutive equation

Herein, we briefly describe the Cam-clay model for finite strain according to Ref. [31, 32]. It is firstly assumed that stretching tensor  $\mathbf{D}$  is divided into elastic and plastic components.

$$\mathbf{D} = \mathbf{D}^e + \mathbf{D}^p \quad (1)$$

The total volume change of the soil skeleton is expressed with the above two terms, namely,

$$\int_0^t J \text{tr} \mathbf{D} d\tau = \int_0^t J \text{tr} \mathbf{D}^e d\tau + \int_0^t J \text{tr} \mathbf{D}^p d\tau \quad (2)$$

where  $J = \det \mathbf{F} = \frac{1+e}{1+e_0}$ ,  $\mathbf{F}$  is the deformation gradient tensor, and  $1+e$  and  $1+e_0$  are the specific volumes at current time  $t$  and reference time  $t=0$ , respectively. The first term in the above equation is written in the following form:

$$\int_0^t J \text{tr} \mathbf{D}^e d\tau = -\frac{\tilde{\kappa}}{1+e_0} \ln \frac{p'}{p'_0} \quad (3)$$

where  $p'$  and  $p'_0$  are the mean effective stresses at the current and the reference states, respectively, and  $\tilde{\kappa}$  is the swelling index.

The total volume change of the soil skeleton should be independent of the stress path, and it is a function of only the initial and the current effective stresses. This is expressed as the sum of the isotropic compression term and the one because of dilatancy:

$$\int_0^t J \text{tr} \mathbf{D} d\tau = -\frac{\tilde{\lambda}}{1+e_0} \ln \frac{p'}{p'_0} + D \frac{q}{p'} = -\frac{\tilde{\lambda}}{1+e_0} \ln \frac{p'}{p'_0} + \frac{\tilde{\lambda} - \tilde{\kappa}}{M(1+e_0)} \frac{q}{p'} \quad (4)$$

where  $\tilde{\lambda}$  is the compression index,  $q$  is the second invariant of deviatoric stress,  $D$  is the dilatancy parameter,  $D = \frac{\tilde{\lambda} - \tilde{\kappa}}{M(1+e_0)}$ , and  $M$  is the critical state parameter.

By subtracting Equation (1) from Equation (2), we have the following well-known Cam-clay yield function:

$$f(p', q) = MD \ln \frac{p'}{p'_0} + D \frac{q}{p'} + \int_0^t J \text{tr} \mathbf{D}^p d\tau \quad (5)$$

The rate type of constitutive equation for the Cam-clay model can be written as

$$\dot{\mathbf{T}}' = \left( \tilde{K} - \frac{2}{3} \tilde{G} \right) (\text{tr} \mathbf{D}) \mathbf{I} + 2 \tilde{G} \mathbf{D} - \frac{\left( \frac{\tilde{G}}{\tilde{\tau}} \mathbf{S} - \tilde{K} \tilde{\beta} \mathbf{I} \right) \left( \frac{\tilde{G}}{\tilde{\tau}} \mathbf{S} \cdot \mathbf{D} - \tilde{K} \tilde{\beta} \text{tr} \mathbf{D} \right)}{\tilde{G} + \tilde{K} \tilde{\beta}^2 + h} \quad (6)$$

where

$$\tilde{K} = \frac{1+e}{\tilde{\kappa}} p', \quad \tilde{G} = \frac{3(1-2\nu)}{2(1+\nu)} \tilde{K}, \quad \tilde{\beta} = \frac{1}{\sqrt{3}} \left( M - \frac{q}{p'} \right), \quad \tilde{\tau} = \frac{q}{\sqrt{3}}, \quad h = \frac{J p' \tilde{\beta}}{\sqrt{3} D}$$

### 3. DATA ASSIMILATION FOR SOIL-WATER COUPLED PROBLEMS

#### 3.1. System equation

The data assimilation technique [33, 34] has been considered in conjunction with the soil-water coupled FEM to identify the elasto-plastic material properties of soil deposits. The following set of system equations is assumed:

$$\mathbf{x}_k = \mathbf{f}_k(\mathbf{x}_{k-1}) + \mathbf{v}_k \quad (7a)$$

$$\mathbf{y}_k = \mathbf{h}_k(\mathbf{x}_k) + \mathbf{\varepsilon}_k \quad (7b)$$

Equation (7a) is the state equation or the system model, and Equation (7b) is the observation equation. Vector  $\mathbf{x}_k$ , called the state vector, includes the state of a system, which is constituted by

the displacement and the pore pressure for soil–water coupled problems at a discrete time  $t = t_k$  ( $k = 1, \dots$ ), whereas vector  $\mathbf{y}_k$ , called the observation vector, indicates the measured quantity. A set of unknown parameters, to be identified based on the measurements, is additionally incorporated into the state vector. Vectors  $\mathbf{v}_k$  and  $\boldsymbol{\varepsilon}_k$  denote system noise and observation noise, respectively, whose probabilistic density function (PDF) follows the normal distribution with an average value of 0, namely,

$$\mathbf{v}_k \approx N(0, \mathbf{Q}_k) \tag{8a}$$

$$\boldsymbol{\varepsilon}_k \approx N(0, \mathbf{R}_k) \tag{8b}$$

where  $\mathbf{Q}_k$  and  $\mathbf{R}_k$  are predetermined covariance matrices.

Operator  $\mathbf{f}_k$  represents the evolution of the states of displacement and pore pressure from time  $t_{k-1}$  to time  $t_k$ , according to the simulation model, that is, the FEM stiffness equation for soil–water coupled problems. Nonlinear function  $\mathbf{h}_k$  describes the measured quantity. In many cases, it is written in matrix form as

$$\mathbf{y}_k = \mathbf{H}_k \mathbf{x}_k + \boldsymbol{\varepsilon}_k \tag{9}$$

where  $\mathbf{H}_k$  is the observation matrix composed of zero or one component, if part of the state variables are directly measured for the geotechnical construction sequence.

### 3.2. Ensemble approximation

Data assimilation strategies based on both the EnKF and the PF employ an ensemble approximation technique where a PDF of stochastic variables is approximated with its realizations and weights. Each realization is called a ‘particle’, and each set is called an ‘ensemble’. For example, the filtered distribution at time  $t = t_{k-1}$ ,  $p(\mathbf{x}_{k-1} | \mathbf{y}_{1:k-1})$ , where  $\mathbf{y}_{1:k-1}$  denotes  $\{\mathbf{y}_1, \mathbf{y}_2, \dots, \mathbf{y}_{k-1}\}$ , is approximated with ensemble  $\{\mathbf{x}_{k-1|k-1}^{(1)}, \mathbf{x}_{k-1|k-1}^{(2)}, \dots, \mathbf{x}_{k-1|k-1}^{(N)}\}$  and weights  $\{w_{k-1}^{(1)}, w_{k-1}^{(2)}, \dots, w_{k-1}^{(N)}\}$  by the following equation:

$$p(\mathbf{x}_{k-1} | \mathbf{y}_{1:k-1}) \approx \sum_{i=1}^N w_{k-1}^{(i)} \delta(\mathbf{x}_{k-1} - \mathbf{x}_{k-1|k-1}^{(i)}) \tag{10}$$

where  $k-1$  represents the index of current time,  $\delta$  is Dirac’s delta function, and  $N$  is the number of particles in the ensemble. In the EnKF and in some kinds of PF (e.g., SIR), each weight  $w_{k-1}^{(i)}$  is set to  $\frac{1}{N}$  in all time steps; as a result, the weight set is omitted.

### 3.3. Prediction and filtering steps for PF and EnKF

3.3.1. *Prediction step for both the EnKF and the PF.* We obtain the ensemble approximation for the predicted distribution  $p(\mathbf{x}_k | \mathbf{y}_{1:k-1})$  at time  $t = t_k$  from the filtered ensemble and weights at time  $t = t_{k-1}$  by the following calculation:

$$\begin{aligned} p(\mathbf{x}_k | \mathbf{y}_{1:k-1}) &= \int p(\mathbf{x}_{k-1} | \mathbf{y}_{1:k-1}) p(\mathbf{x}_k | \mathbf{x}_{k-1}) d\mathbf{x}_{k-1} \\ &\approx \sum_{i=1}^N \int w_{k-1}^{(i)} \delta(\mathbf{x}_{k-1} - \mathbf{x}_{k-1|k-1}^{(i)}) p(\mathbf{x}_k | \mathbf{x}_{k-1}) d\mathbf{x}_{k-1} \\ &= \sum_{i=1}^N w_{k-1}^{(i)} \delta(\mathbf{x}_k - (\mathbf{f}_k(\mathbf{x}_{k-1|k-1}^{(i)}) + \mathbf{v}_k^{(i)})) \\ &= \sum_{i=1}^N w_{k-1}^{(i)} \delta(\mathbf{x}_k - \mathbf{x}_{k|k-1}^{(i)}), \end{aligned} \tag{11}$$

where  $\{\mathbf{v}_k^{(i)}\}_{i=1}^N$  is an i.i.d. (independent and identically distributed) sample set of Equation (8a). This calculation means that each particle for the prediction ensemble,  $\mathbf{x}_{k|k-1}^{(i)}$ , is generated via the state

equation (Equation (7a)), that is, the stiffness equation for the soil–water coupled FEM appearing in the previous chapter for geotechnical applications

$$\mathbf{x}_{k|k-1}^{(i)} = \mathbf{f}_k \left( \mathbf{x}_{k-1|k-1}^{(i)} \right) + \mathbf{v}_k^{(i)} \quad (12)$$

and the weights are unchanged in this step.

3.3.2. *Filtering step for the EnKF.* Sample mean  $\hat{\mathbf{x}}_{k|k-1}$  and sample covariance matrix  $\hat{\mathbf{V}}_{k|k-1}$  are computed as follows:

$$\hat{\mathbf{x}}_{k|k-1} = \frac{1}{N} \sum_{i=1}^N \mathbf{x}_{k|k-1}^{(i)} \quad (13)$$

$$\hat{\mathbf{V}}_{k|k-1} = \frac{1}{N-1} \sum_{i=1}^N \left( \mathbf{x}_{k|k-1}^{(i)} - \hat{\mathbf{x}}_{k|k-1} \right) \left( \mathbf{x}_{k|k-1}^{(i)} - \hat{\mathbf{x}}_{k|k-1} \right)^T \quad (14)$$

The filtered ensemble is obtained through the updated equation of the usual Kalman filtering, namely,

$$\mathbf{K}_k = \hat{\mathbf{V}}_{k|k-1} \mathbf{H}_k^T \left( \mathbf{H}_k \hat{\mathbf{V}}_{k|k-1} \mathbf{H}_k^T + \mathbf{R}_k \right)^{-1} \quad (15)$$

$$\mathbf{x}_{k|k}^{(i)} = \mathbf{x}_{k|k-1}^{(i)} + \mathbf{K}_k \left( \mathbf{y}_k - \mathbf{H}_k \mathbf{x}_{k|k-1}^{(i)} + \boldsymbol{\varepsilon}_k^{(i)} \right) \quad (16)$$

where  $\left\{ \boldsymbol{\varepsilon}_k^{(i)} \right\}_{i=1}^N$  is an i.i.d., independent and identically distributed, sample set of Equation (8b). As mentioned above, the weight set is not required because particles still have an equal weight after the calculation of the filtered ensemble in the EnKF.

3.3.3. *Filtering step for the PF.* We obtain an approximation of the filtered distribution,  $p(\mathbf{x}_k | \mathbf{y}_{1:k})$ , from the ensemble of the predicted distribution,  $p(\mathbf{x}_k | \mathbf{y}_{1:k-1})$ , and observation  $\mathbf{y}_k$  using the Bayes' theorem, namely,

$$\begin{aligned} p(\mathbf{x}_k | \mathbf{y}_{1:k}) &= \frac{p(\mathbf{x}_k | \mathbf{y}_{1:k-1}) p(\mathbf{y}_k | \mathbf{x}_k)}{\int p(\mathbf{x}_k | \mathbf{y}_{1:k-1}) p(\mathbf{y}_k | \mathbf{x}_k) d\mathbf{x}_k} \\ &\approx \frac{1}{\sum_j p(\mathbf{y}_k | \mathbf{x}_{k|k-1}^{(j)}) w_{k-1}^{(j)}} \sum_{i=1}^N p(\mathbf{y}_k | \mathbf{x}_{k|k-1}^{(i)}) w_{k-1}^{(i)} \delta(\mathbf{x}_k - \mathbf{x}_{k|k-1}^{(i)}) \\ &= \sum_{i=1}^N s_i w_{k-1}^{(i)} \delta(\mathbf{x}_k - \mathbf{x}_{k|k-1}^{(i)}) \\ &= \sum_{i=1}^N w_k^{(i)} \delta(\mathbf{x}_k - \mathbf{x}_{k|k-1}^{(i)}) \end{aligned} \quad (17)$$

where  $s_i$  is defined as

$$s_i = \frac{p(\mathbf{y}_k | \mathbf{x}_{k|k-1}^{(i)})}{\sum_j p(\mathbf{y}_k | \mathbf{x}_{k|k-1}^{(j)}) w_{k-1}^{(j)}} \quad (18)$$

and is calculated in the following manner in the case of linear observations:

$$p(\mathbf{y}_k | \mathbf{x}_{k|k-1}^{(i)}) = \frac{1}{\sqrt{(2\pi)^m |\mathbf{R}_k|}} \exp \left[ -\frac{\left( \mathbf{y}_k - \mathbf{H}_k \mathbf{x}_{k|k-1}^{(i)} \right)^T \mathbf{R}_k^{-1} \left( \mathbf{y}_k - \mathbf{H}_k \mathbf{x}_{k|k-1}^{(i)} \right)}{2} \right]. \quad (19)$$

Each weight  $w_k^{(i)}$  is the product of  $s_i$  and the previous time weight,  $w_{k-1}^{(i)}$ , namely,

$$w_k^{(i)} = s_i w_{k-1}^{(i)} \tag{20}$$

The sampling importance resampling (SIR) algorithm, one of the PF procedures, proceeds in the following steps:

1) Initialization:

Draw a sample of size  $N$  from the prior density at the initial time and define the sample set as  $\{\mathbf{x}_{0|0}^{(i)}\}$ .

2) Preliminaries:

Assume that  $\{\mathbf{x}_{k-1|k-1}^{(i)}\}$  is a population of  $N$  particles, approximately distributed as in an independent sample from  $p(\mathbf{x}_{k-1}|\mathbf{y}_{1:k-1})$ .

3) Prediction:

Sample  $N$  values,  $\mathbf{v}_k^{(i)}$ , from the distribution of  $\mathbf{v}_k$ . Use these to generate a new population of particles,  $\{\mathbf{x}_{k|k-1}^{(i)}\}$ , via Equation (17).

4) Filtering:

Assign a weight  $s_i$  to each  $\mathbf{x}_{k|k-1}^{(i)}$ . This weight is calculated by Equation (18).

5) Resampling:

Resample  $N$  times with replacement from the set of particles  $\{\mathbf{x}_{k|k-1}^{(i)}\}$ , which is obtained in the filtering stage, with the probability proportional to  $s_i$ . The set of determined particles,  $\{\mathbf{x}_{k|k}^{(i)}\}$ , results in an ensemble approximation of  $p(\mathbf{x}_k|\mathbf{y}_{1:k})$ .

In this procedure, weight set  $\{w_k^{(i)}\}$  is not required because the resampling flattens the weight difference among the particles and resets it to  $\frac{1}{N}$ .

On the other hand, filtering via sequential importance sampling (SIS) [35, 36] preserves the weight set  $\{w_k^{(i)}\}$  and calculates  $w_k^{(i)}$  by Equation (20) instead of by resampling. Initial weight  $w_0^{(i)}$  is usually set to  $\frac{1}{N}$ , see Figure 3.

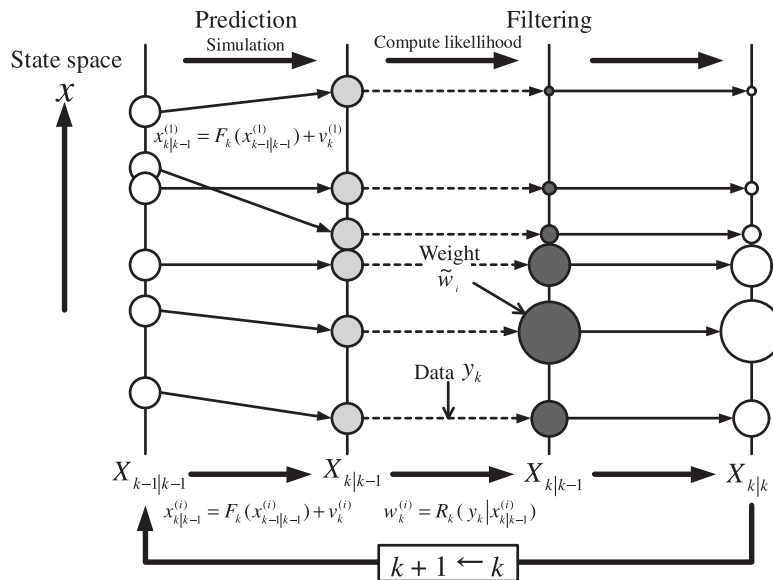


Figure 3. Computational procedure of the particle filter with sequential importance sampling.

To identify the elasto-plastic material properties of geomaterials, the PF without resampling, that is, SIS, is adopted as the preferable tool for analyzing numerical examples. This is because, within the framework of the EnKF, Equation (16) adjusts the state vector consisting of the displacement, the pore pressure, and the parameters to be identified based on each observation, and then, the resultant stiffness matrix constructed by the resampled displacement and pre-pressure leads to numerical predictions with less accuracy.

Prior to the filtering, a sufficient number of samples for a set of parameters to be identified is scattered over the prescribed range so as to cover their possible values, and its weighted average is the initial value of each parameter for identification. Numerical simulations are carried out using each sample, and the computed quantity corresponding to the measured one is incorporated into the evaluation of likelihood at each step of the observation. However, an iterative method seeking the minimum or the maximum of a nonlinear objective function is not necessary.

#### 4. NUMERICAL ANALYSES FOR SOIL–WATER COUPLED PROBLEMS

##### 4.1. Soil element tests

As the first example, to examine the numerical accuracy of the computational procedure described in the previous sections, hypothetical drained and undrained soil element tests are analyzed under plane strain conditions, as can be seen in the schematic description in Figure 4. Soil tests were numerically carried out by a synthetic soil–water FEM using the set of parameters listed in Table III, assuming a clayey specimen with a plasticity index of around 30. Compression index  $\lambda$ , swelling index  $\kappa$ , critical state parameter  $M$ , and initial mean effective stress  $p_0'$ , among the Cam-clay parameters, are identified based on the vertical displacement measurements at the top of the specimen,  $\delta_y$ , during the loading process shown in Figure 5. System noise is assumed to be zero throughout the subsequent problems.

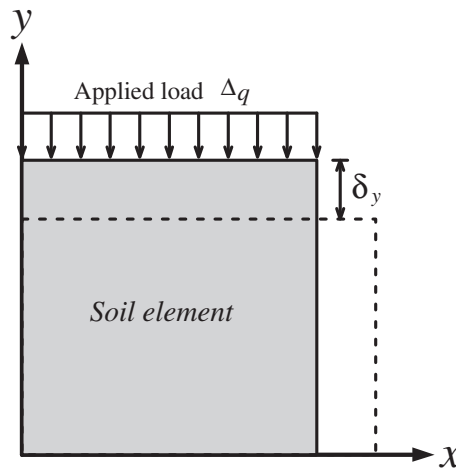


Figure 4. Schematic illustration of the soil tests.

Table III. Parameters of the Cam-clay model used in analyzing the soil tests.

$\nu$	$\lambda$	$\kappa$	$e_0$	$M$	$K_0$	$p_0'$ (kPa)
0.333	0.225	0.083	1.087	1.103	1.00	98.0

Table IV describes the range in parameters in which particles are generated using uniform random numbers. This set of parameters, except for the initial stress, corresponds to that of clayey soil with a plasticity index of 10 to 50. Table V classifies the 15 cases to be analyzed, where more numbers of particles are adopted for more numbers of unknowns, and the diagonal terms of the error covariance matrix are assumed as the following term with parameter  $\alpha$ :

$$R_{ij} = (\alpha S_{\max})^2 \delta_{ij} \tag{21}$$

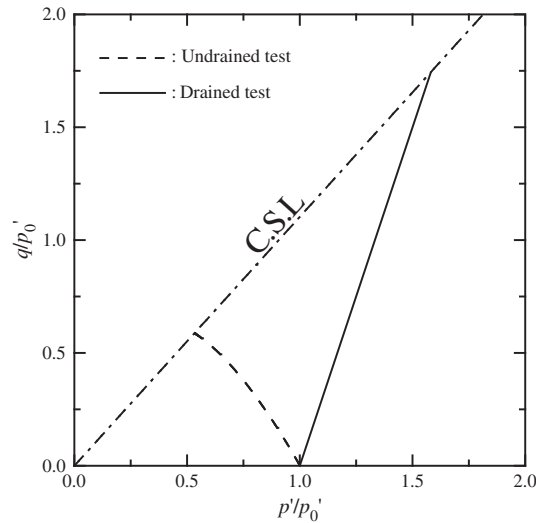


Figure 5. Effective stress paths during the drained and undrained shear tests.

Table IV. Range in particle generation.

Parameter	Range in particle generation
$\lambda$	$0.085 \leq \lambda \leq 0.435$
$\kappa$	$0.016 \leq \kappa \leq 0.208$
$M$	$0.912 \leq M \leq 1.429$
$p_0'$ (kPa)	$60.0 \leq p_0' \leq 140.0$

Table V. Cases to be analyzed.

	Parameters to be identified	Number of particles	$\alpha$ (%)
Case 1	$\lambda$	300	30.0
Case 2	$\kappa$		
Case 3	$M$		
Case 4	$p_0'$		
Case 5	$\lambda, \kappa$	600	
Case 6	$\lambda, M$		
Case 7	$\lambda, p_0'$		
Case 8	$\kappa, M$		
Case 9	$\kappa, p_0'$	1200	
Case 10	$M, p_0'$		
Case 11	$\lambda, \kappa, M$		
Case 12	$\lambda, \kappa, p_0'$		
Case 13	$\lambda, M, p_0'$	2400	
Case 14	$\kappa, M, p_0'$		
Case 15	$\lambda, \kappa, M, p_0'$		

where  $R_{ij}$  is the error covariance matrix for the observation,  $S_{\max}$  is the presumed maximum settlement,  $\delta_{ij}$  is Kronecker's delta, and  $\alpha$  is assumed to be 30% in all cases.

Tables VI and VII list the identified parameters for each case in Table V at the end of the observations for the undrained and the drained element tests, respectively, and Figures 6 and 7 show the identification process of the parameters corresponding to Tables VI and VII, respectively, where the identified parameters at each time step are obtained by the weighted average of the samples. It is revealed from Figure 6 that for almost all the cases of the undrained tests, except for Case 15, which includes four unknown parameters, the identification of one or two unknown parameters is provided with high accuracy. From Figure 7, on the other hand, the numerical results of Cases 15 and 14, including three unknown parameters for the drained tests, are less accurate than those for the undrained tests. The stress path of the undrained shear has the shape of a nonlinear curve and expresses the yielding surface well, as shown in Figure 5, whereas that of the drained shear is a simple linear line. Namely, the undrained stress path is more informative for the shape of the yielding surface, and consequently, the elasto-plastic parameters are easier to be identified in the undrained shear than in the drained shear. However, there are some difficulties in obtaining

Table VI. Identified parameters for the undrained tests.

	$\lambda$	$\kappa$	M	$p'_0$ (kPa)
Correct	0.225	0.083	1.103	98.0
Case 1	0.226	—	—	—
Case 2	—	0.085	—	—
Case 3	—	—	1.104	-
Case 4	—	—	—	98.0
Case 5	0.222	0.080	—	—
Case 6	0.248	—	1.105	—
Case 7	0.276	—	—	101.9
Case 8	—	0.086	1.088	-
Case 9	—	0.084	—	98.2
Case 10	—	—	1.114	98.2
Case 11	0.311	0.084	1.200	—
Case 12	0.264	0.085	—	99.3
Case 13	0.303	—	1.144	101.6
Case 14	—	0.086	1.132	96.2
Case 15	0.302	0.084	1.132	101.6

Table VII. Identified parameters for the drained tests.

	$\lambda$	$\kappa$	M	$p'_0$ (kPa)
Correct	0.225	0.083	1.103	98.0
Case 1	0.225	—	—	—
Case 2	—	0.089	—	—
Case 3	—	—	1.105	—
Case 4	—	—	—	98.1
Case 5	0.222	0.097	—	—
Case 6	0.233	—	1.155	—
Case 7	0.262	—	—	117.6
Case 8	—	0.086	1.100	—
Case 9	—	0.085	—	98.4
Case 10	—	—	1.212	91.5
Case 11	0.250	0.115	1.257	—
Case 12	0.263	0.105	—	117.9
Case 13	0.271	—	1.209	115.2
Case 14	—	0.093	1.161	94.6
Case 15	0.279	0.116	1.247	114.9

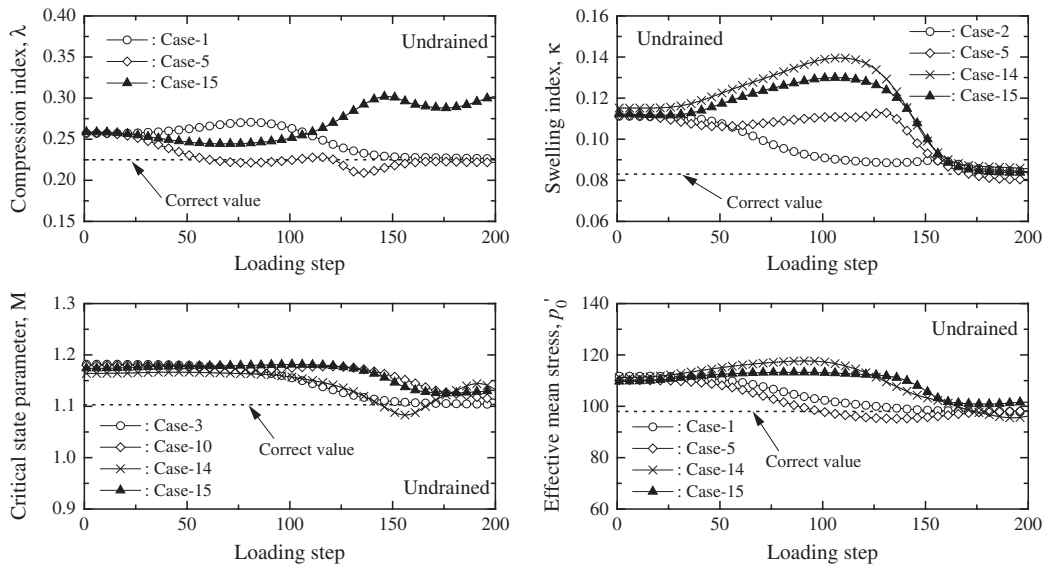


Figure 6. Identification of parameters for undrained tests.

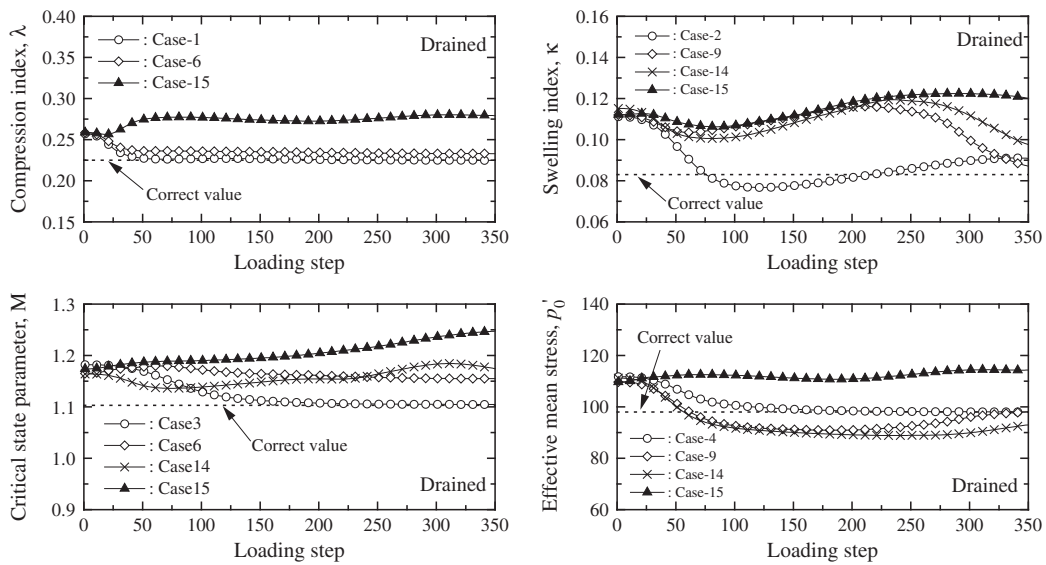


Figure 7. Identification of parameters for drained tests.

solutions with high accuracy in the case of four unknown parameters irrespective of whether the tests are undrained or drained within a given number of particles, observation, and error covariance.

#### 4.2. Soil deposit under embankment loading

We also examine the performance of the PF with FEM for the hypothetical soil deposit under continuous embankment loading. Figure 8 presents a description of the problem under consideration, the finite element mesh, and the boundary conditions used in the analysis. The embankment is assumed to be constructed according to the schedule in Figure 9 on a foundation ground, which consists of a homogeneous clay layer; its parameters for the Cam-clay model are listed in Table VIII. At the points depicted in Figure 10, the measurements of the settlement are synthetically simulated based on the soil–water coupled FEM computation and seeded by random numbers of 5% white noise of the maximum measurement for Case 1 as seen in Figure 11.

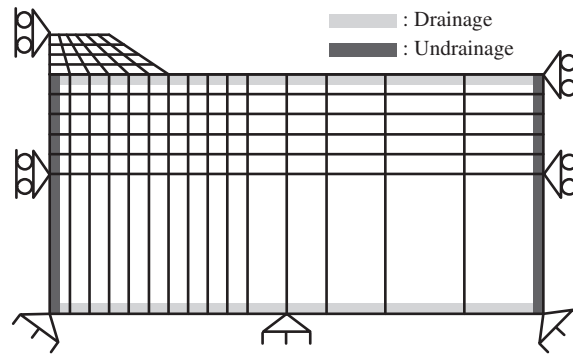


Figure 8. Description of soil deposit under embankment loading.

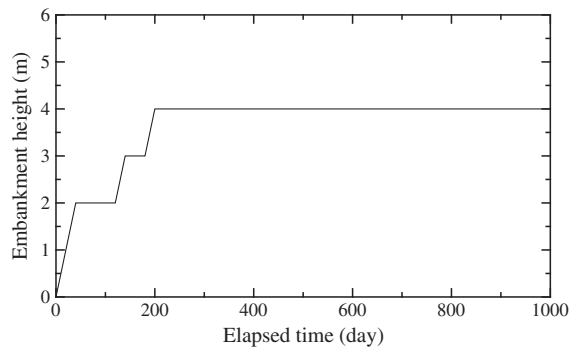


Figure 9. History of embankment loading.

Table VIII. Parameters of the Cam-clay model for embankment foundation.

$\nu$	$\lambda$	$\kappa$	$e_0$	$M$	$K_0$	$p_0'$ (kPa)	$k_{v0}$ (m/day)	$\lambda_k$
0.333	0.330	0.143	1.372	0.990	1.00	150.0	$6.05 \times 10^{-4}$	0.928

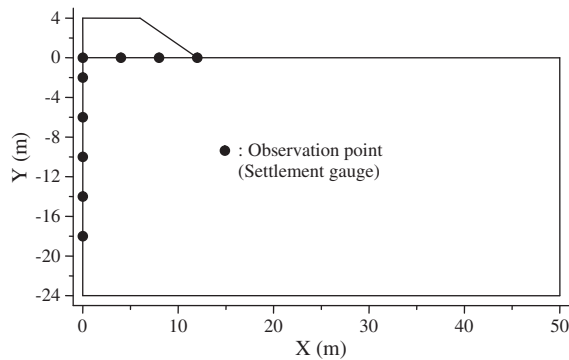


Figure 10. Allocation of devices for settlement measurement.

Table IX describes six cases of three unknown parameters to be identified among the quantities listed in Table VIII under the same level of error covariance,  $\alpha$ , of 30%, as shown in Table V, where 2000 particles are generated and fall within the range for each unknown in Table X based on uniform random numbers.

Table XI lists the identified parameters during the 1,000 days of observation. The identification process over the elapsed time in Figure 12 reveals that the permeability can easily be identified, whereas the initial stress can hardly be identified. The identification process over the elapsed time in

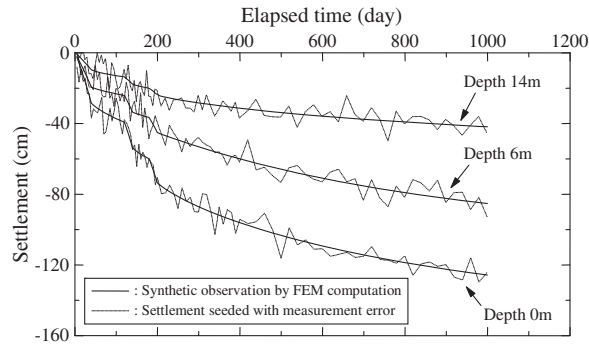


Figure 11. Settlement measurement seeded by random numbers.

Table IX. Cases to be identified.

	Parameters to be identified	Number of particles	$\alpha$ (%)
Case 1	$\lambda, \kappa, k$	2000	30.0
Case 2	$\lambda, M, k$		
Case 3	$\lambda, p_0', k$		
Case 4	$\kappa, M, k$		
Case 5	$\kappa, p_0', k$		
Case 6	$M, p_0', k$		

Table X. Range in particle generation.

Parameter	Range in particle generation
$\lambda$	$0.155 \leq \lambda \leq 0.435$
$\kappa$	$0.047 \leq \kappa \leq 0.208$
$M$	$0.912 \leq M \leq 1.220$
$p_0'$ (kPa)	$100.0 \leq p_0' \leq 180.0$
$k_{v0}$ (m/day)	$1.0 \times 10^{-1} \leq k_{v0} \leq 1.00 \times 10^{-7}$

Table XI. Identified parameters for the soil deposit.

	$\lambda$	$\kappa$	$M$	$p_0'$ (kPa)	$k_{v0}$ (m/day)
Correct	0.330	0.143	0.990	150.0	$6.05 \times 10^{-4}$
Case 1	0.328	0.147	—	—	$6.08 \times 10^{-4}$
Case 2	0.306	—	1.000	—	$6.50 \times 10^{-4}$
Case 3	0.310	—	—	143.1	$6.36 \times 10^{-4}$
Case 4	—	0.131	1.000	—	$7.04 \times 10^{-4}$
Case 5	—	0.138	—	133.6	$6.15 \times 10^{-4}$
Case 6	—	—	1.066	131.0	$6.15 \times 10^{-4}$

Figure 12 reveals that the permeability can easily be identified, whereas the initial stress can hardly be identified. Permeability can easily be identified in comparison with other parameters because it relates to the settlement rate. Figure 13 compares the identification of the parameters for Case 1 between seeded with or without a random noise of 5% to examine the effect of the measurement noise. From a practical viewpoint, the PF is a robust tool, which is advantageous in identifying the parameters for contaminant measurements with noise.

Figure 14 depicts the distribution of weight for each unknown parameter in Case 1 at different time stages, namely, compression index, swelling index, and permeability. It can be seen from Figure 14 that the weight for the permeability approximately follows the normal distribution around the prescribed value producing the hypothetical observation and that for the compression index and the swelling index has a similar distribution, which is not sharply shaped around the prescribed one. It

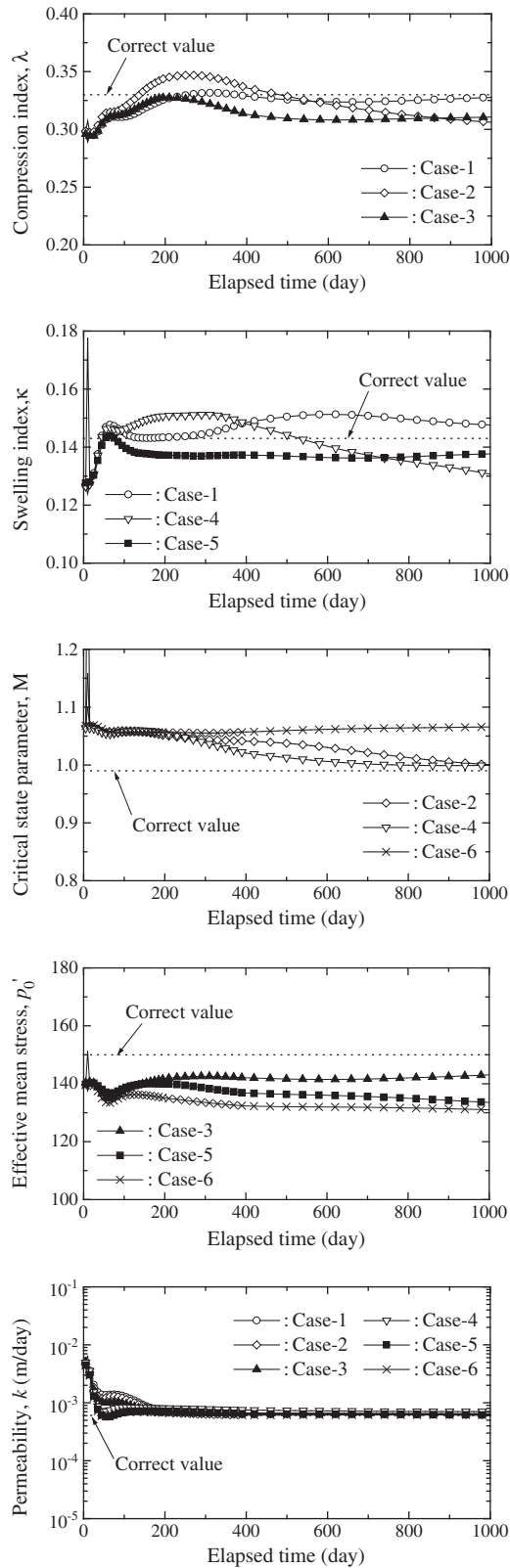


Figure 12. Identification of parameters for soil deposit.

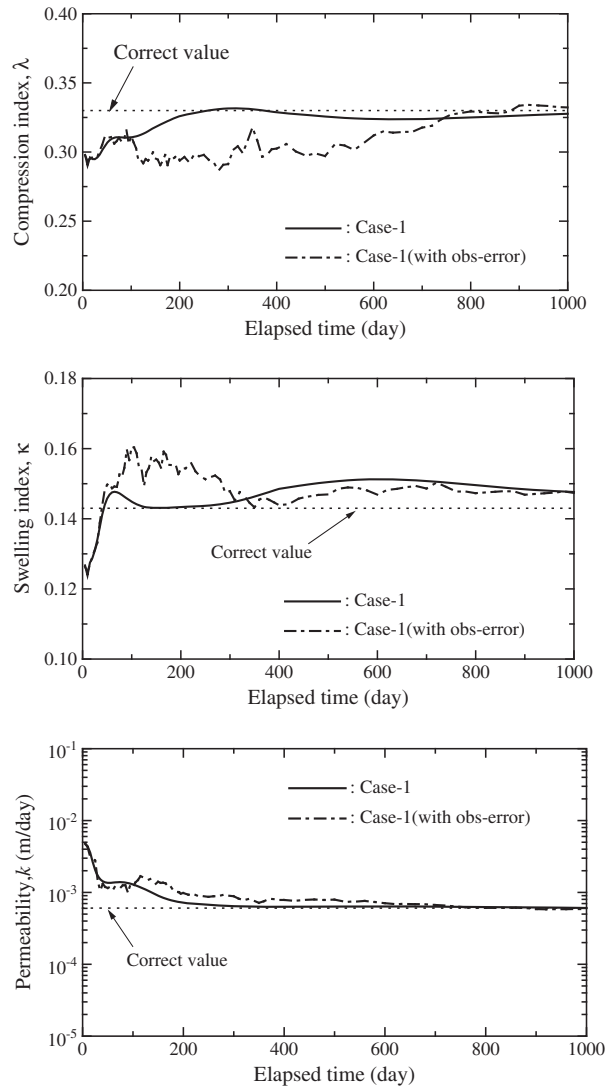
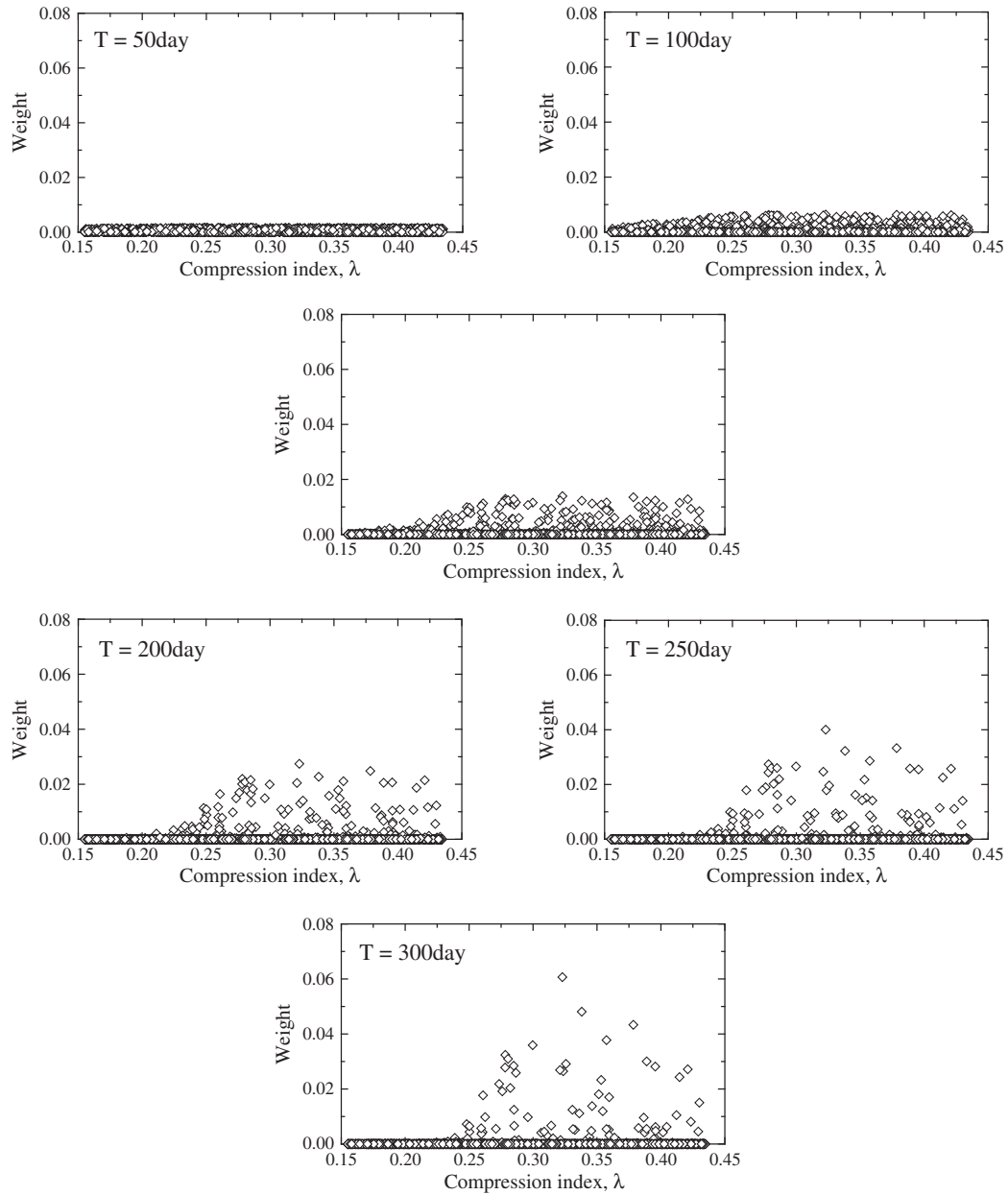


Figure 13. Comparison of parameter identification for Case 1 between seeded with or without measurement noise.

can be seen from Figure 14 that the weight for the permeability approximately follows the normal distribution around the prescribed value producing the hypothetical observation and that for the compression index and the swelling index have a similar distribution, which is mildly convex around the prescribed one. These resultant weight distributions have a unimodal shape with one peak and lead to a more highly accurate identification.

## 5. APPLICATION OF THE PF TO GEOTECHNICAL PRACTICES

This chapter presents an example application of the PF to the actual settlement prediction of a well-documented geotechnical construction project, Kobe Airport Island. First, the geotechnical parameters of the actual ground are identified using the methodology presented in the previous chapter. Then, by comparing the recomputed simulation, using the identified parameters, with the observation data, the practical effectiveness of the methodology based on the PF is discussed. Some outcomes obtained from this application have been reported in Ref. [37].



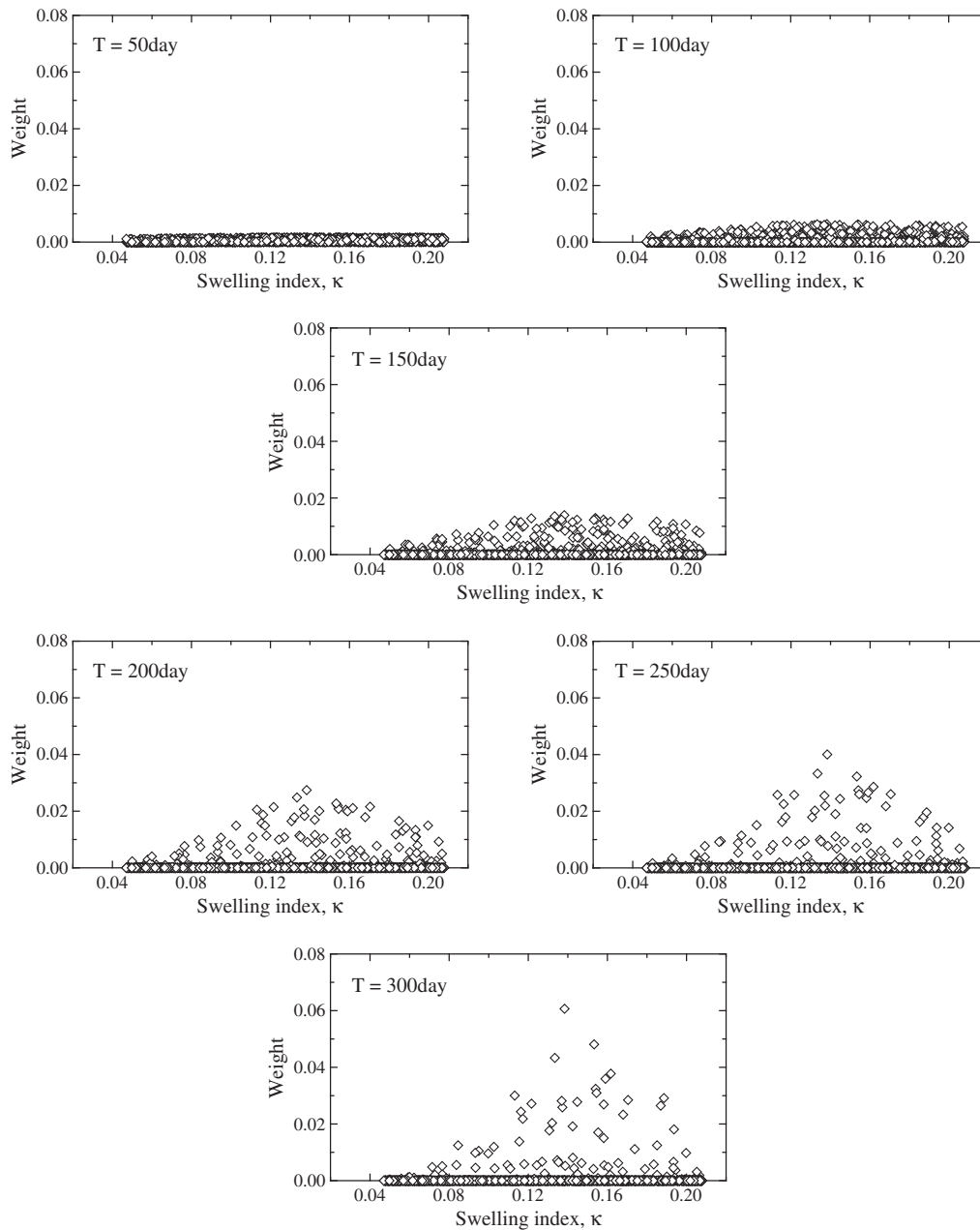
(a) Compression index

Figure 14. Distribution of weight for each unknown parameter at different time stages.

Kobe Airport was constructed on an artificially reclaimed island just off the coast of Kobe City, Japan. Figure 15 shows the cross section of the construction site. Vertical sand drains were installed in the soft clay layer to accelerate the settlement and to increase the strength (e.g., [38, 39]).

The construction site is located on a soft marine clay deposit; therefore, several instruments were placed around the site to monitor the settlement and the lateral displacement of the seawall and the foundation ground. These instruments included inclinometers at the toe of the seawall, settlement plates and earth pressure gauges on the seabed, and pore pressure meters on each soil layer. The cross section of the site and the placement of the instruments are shown in Figures 15 and 16, respectively.

A soil–water coupled finite element analysis, with the Cam-clay model, was adopted for analyzing the deformation behavior of the seawall and the foundation subjected to the construction and

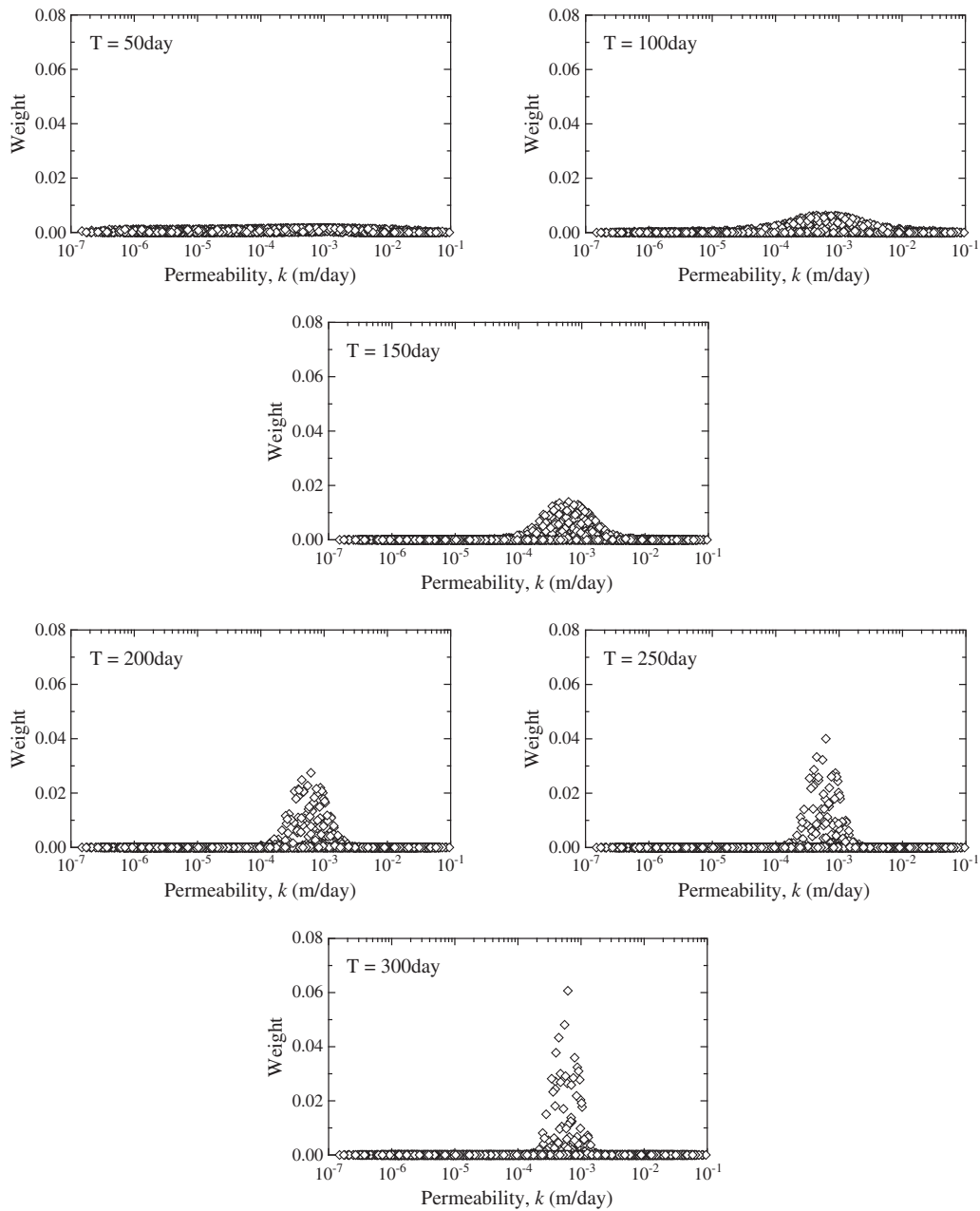


(b) Swelling index

Figure 14. *Continued*

reclamation work. Figure 17 shows the finite element mesh used in this analysis. In the model ground, the top surface, the bottom surface, and the sides of the sand/gravel layers were assumed to have permeable boundary conditions, whereas the sides of the clay layers were assumed to have impermeable boundary conditions. The sand layers and the reclaimed ground were assumed to be linear elastic, and the clay foundations were represented by the Cam-clay model.

The *mass permeability* concept, which was proposed by [40], was incorporated into this analysis. Mass permeability is the permeability representative of a clay foundation, which includes the effects of inhomogeneity, partial drainage, and load intensity. We also adopted the concept in the same sense. The analysis in this chapter focuses on the settlement behavior of only the improved alluvial clay foundation because the soil layers, which are just below the improved ground, called Ds1-Ds3,



**(c) Coefficient of permeability**

Figure 14. *Continued*

are thick, have high rigidity (the N-value obtained from SPT is more than 100), and do not significantly affect the settlement of the island.

First, we considered the improved ground to be homogeneous by incorporating the mass permeability concept. Then, using the PF, some parameters of the treated ground, the *mass parameters*, were identified to simulate the settlement of the ground under the airport island. Although some of the parameters listed in Table XII affect the settlement of the ground, compression index  $\lambda$  and permeability  $k$  were treated as the only parameters to be identified. This is because these two parameters directly govern the consolidation behavior of clay grounds. Finally, the simulations were implemented using the identified mass parameters, and the observation data were compared to evaluate the practical usability of the PF.

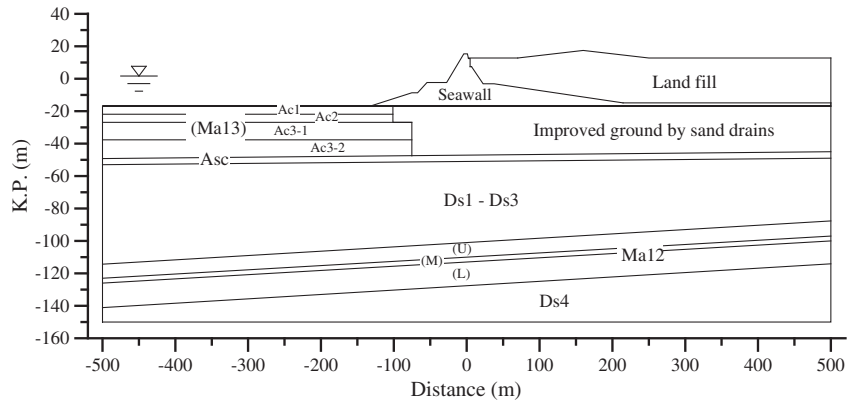


Figure 15. Cross section of the construction site (modified from Ref. [38]).

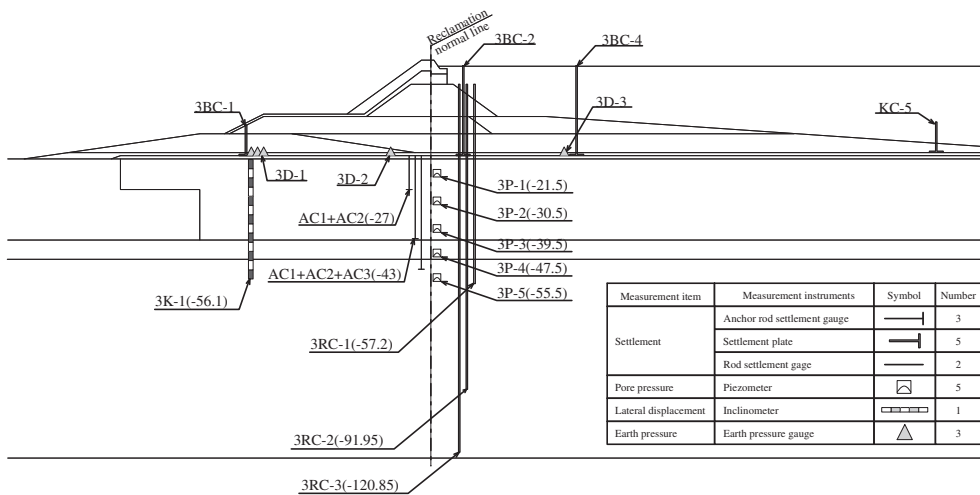


Figure 16. Location of measurement instruments (modified from Ref. [39]).

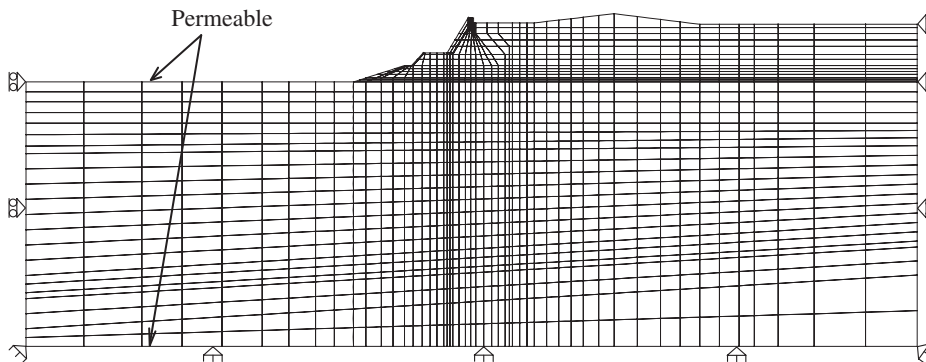


Figure 17. Problem description.

Table XII. Parameters of the foundation ground for finite element model (modified from Ref. [31]).

Soil layer	$\nu$	$\lambda$	$\kappa$	$e_i$	M	$k$ (m/day)	$\lambda_k$	$K_i$	OCR
AC1	0.300	0.304	0.098	2.473	1.187	$5.17 \times 10^{-4}$ ( $5.38 \times 10^{-2}$ )	0.304	0.868 (1.000)	1.46 (1.00)
AC2	0.300	0.313	0.113	2.150	1.117	$2.00 \times 10^{-4}$ ( $2.06 \times 10^{-2}$ )	0.313	0.790 (1.000)	1.41 (1.00)
AC3-1(1)	0.300	0.339	0.115	2.037	1.157	$1.43 \times 10^{-4}$ ( $1.45 \times 10^{-2}$ )	0.339	0.773 (1.000)	1.36 (1.00)
AC3-1(2)	0.300	0.321	0.094	1.851	1.239	$1.06 \times 10^{-4}$ ( $1.05 \times 10^{-2}$ )	0.321	0.750 (1.000)	1.33 (1.00)
AC3-2(1)	0.300	0.365	0.124	1.924	1.157	$9.42 \times 10^{-5}$ ( $8.44 \times 10^{-2}$ )	0.365	0.729 (1.000)	1.20 (1.00)
AC3-2(2)	0.300	0.378	0.152	1.975	1.044	$7.98 \times 10^{-5}$ ( $7.07 \times 10^{-2}$ )	0.378	0.746 (1.000)	1.19 (1.00)
AC3-2(3)	0.300	0.387	0.123	1.876	1.191	$7.42 \times 10^{-5}$ ( $6.55 \times 10^{-2}$ )	0.387	0.719 (1.000)	1.19 (1.00)
ASC	0.300	0.239	0.077	1.350	1.183	$3.48 \times 10^{-5}$	0.239	0.780	1.59
DS1	0.300		$E = 14\,000\text{ kN/m}^2$			$8.64 \times 10^{-1}$	—	—	—
DS2	0.300		$E = 63\,000\text{ kN/m}^2$			$8.64 \times 10^{-1}$	—	—	—
DS3	0.300		$E = 28\,000\text{ kN/m}^2$			$8.64 \times 10^{-1}$	—	—	—
MA12U	0.300	0.300	0.113	1.359	1.091	$2.42 \times 10^{-5}$	0.300	0.813	1.48
MA12M	0.300	0.256	0.085	1.158	1.170	$2.91 \times 10^{-5}$	0.256	0.737	1.28
MA12L	0.300	0.295	0.113	1.251	1.083	$1.64 \times 10^{-5}$	0.259	0.816	1.50
DS4	0.300		$E = 1\,000\,000\text{ kN/m}^2$			$4.32 \times 10^{-1}$	—	—	—

The representative parameters of the improved grounds, referred to as mass parameters ( $P_{\text{mass}}$ ) in this study, are determined here with Equation (22) for simplicity.

$$P_{\text{mass}} = \frac{P_1 h_1 + P_2 h_2 + \dots + P_n h_n}{h_1 + h_2 + \dots + h_n} \quad (22)$$

where  $P_i$ ,  $h_i$  ( $i = 1, 2, \dots, n$ ), and  $n$  are the parameters, the thickness of each layer, and the number of soil layers, respectively.

We conducted Monte Carlo simulations with 200 particles over the feasible space listed in Table XIII. Each parameter was assumed to follow uniform randomness and was generated independently. All 200 simulations were conducted up to 676 days after the construction was started. Only the settlement values observed on the seabed (3BC-2, 3BC-4, and KC-5) were used for parameter identification.

Figure 18 shows the time evolution of the identified parameters. As seen in Figure 18(a), estimates for  $\lambda$  hardly change throughout the assimilation. In particular, after the 300th day, the path changes dramatically. On the other hand, in the results shown in Figure 18(b) for  $k$ , the identified parameter shows an almost constant value throughout the assimilation.

The simulation results for the time-settlement relationship at observation points 3BC-2 and 3BC-4, which were placed on the seabed, via the identified parameters, are shown in Figure 19(a) and (b), respectively. The identified parameters mean the values at the end of the identification process, that is,  $t = 456$  days. In the figures, the dotted line represents the results of the direct analysis using the geotechnical parameters listed in Table XII. Although the results of the direct analysis underestimate the observation data, the simulations using the identified parameters (DA) yielded predictions with high accuracy.

Table XIII. Range in particle generation.

Parameter	Range in particle generation
$\lambda$	$0.30 \leq \lambda \leq 0.60$
$k$ (m/day)	$1 \times 10^{-0} \leq k \leq 1 \times 10^{-3}$

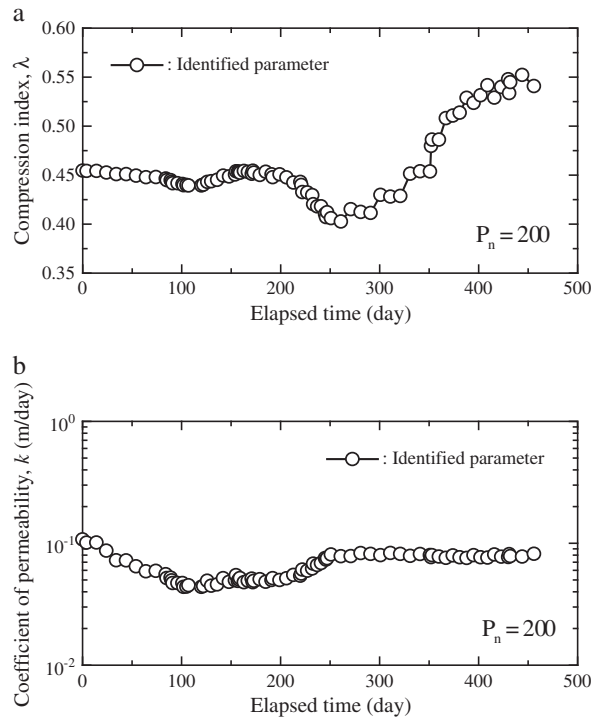


Figure 18. Time evolution of identified parameters.

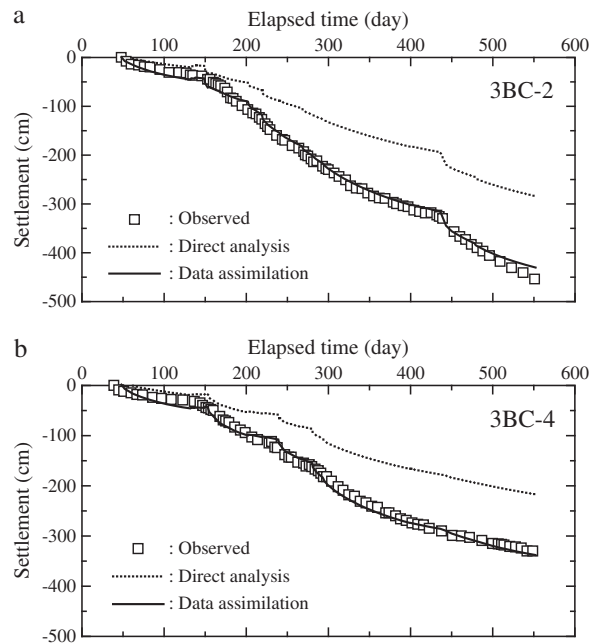


Figure 19. Simulation results using the identified parameters.

## 6. CONCLUSIONS

This paper has introduced a computational procedure for data assimilation using the PF in conjunction with a soil–water coupled FEM to identify a set of parameters for the elasto-plastic constitutive model for geomaterials based on measurements. The stiffness equation for a soil–water coupled FEM, incorporating the Cam-clay model, corresponds to the state equation of the PF, and the observation

equation denotes the location of the measurements among the FEM nodes. The SIS, one of the PF procedures without resampling, is adopted for identification in elasto-plastic problems.

To examine the validity of the proposed procedure, the SIS with a soil–water coupled FEM is applied to synthetic observed data for the settlement in hypothetical soil element tests and to the soil deposit under embankment loading which is generated by a synthetic FEM using the prescribed values for a couple of parameters to be known a priori in the data assimilation. For both cases, the identified parameters are in good agreement with the prescribed values used in the prior FEM computation for generating the synthetic measurements irrespective of the artificial measurement error.

The PF has also been applied to the actual settlement predictions of Kobe Airport Island, and the effectiveness has been discussed comparing the assimilation results and the corresponding observation data. Application of the PF to practical problems can include several technical issues, which arise from computational costs and the lack of observation data. To tackle the above issues, the *mass permeability* concept was incorporated in the assimilation, and the representative parameters of the treated ground by sand drains, the so-called *mass parameter*, were identified. The simulation results using the identified parameters agreed well the actual observation data, and they suggest that the DA using the PF is a highly effective approach for geotechnical analysis.

It appears that sequential data assimilation techniques, such as the particle filter, are the preferable tools that can provide estimates of the state variables, that is, deformation, pore pressure, and unknown parameters, for the constitutive model in geotechnical practice.

#### APPENDIX A: GOVERNING EQUATIONS FOR SOIL-WATER COUPLED PROBLEM

a) Continuous equilibrium equation

$$\int_V \text{div} \dot{\mathbf{S}}_t dV = 0, \dot{\mathbf{S}}_t = \dot{\mathbf{T}} + (\text{tr} \mathbf{D}) \mathbf{T} - \mathbf{T} \mathbf{L}^T \quad (\text{A.1})$$

where  $\dot{\mathbf{S}}_t$  is the nominal stress rate,  $\mathbf{T}$  is the total Cauchy stress,  $\dot{\mathbf{T}}$  is the Cauchy stress rate,  $\mathbf{L}$  is the velocity gradient,  $\mathbf{D}$  is the stretching, and  $V$  is the domain. Equation (A.1) is written in the following local form because of the arbitrariness of the domain:

$$\text{div} \dot{\mathbf{S}}_t = 0, \dot{\mathbf{S}}_t = \dot{\mathbf{T}} + (\text{tr} \mathbf{D}) \mathbf{T} - \mathbf{T} \mathbf{L}^T \quad (\text{A.2})$$

b) Effective stress concept

$$\mathbf{T} = \mathbf{T}' - p_w \mathbf{I} \quad (\text{A.3})$$

where  $\mathbf{T}'$  is the effective stress,  $p_w$  is the pore water pressure, and  $\mathbf{I}$  is the unit tensor.

c) Constitutive equation

$$\overset{\circ}{\mathbf{T}}' = \mathbf{L}[\mathbf{D}] \quad (\text{A.4})$$

where  $\overset{\circ}{\mathbf{T}}'$  is the Jaumann rate of the effective stress in the form of

$$\overset{\circ}{\mathbf{T}}' = \dot{\mathbf{T}}' - \mathbf{W} \mathbf{T}' + \mathbf{T}' \mathbf{W} \quad (\text{A.5})$$

where  $\dot{\mathbf{T}}'$  is the effective Cauchy stress rate and  $\mathbf{W}$  is the spin tensor.

d) Continuity condition of soil–water coupled problems

$$\text{tr} \mathbf{D} + \text{div} \mathbf{v}_w = 0 \quad (\text{A.6})$$

where  $\mathbf{v}_w$  is the average velocity of the pore water and the above equation is derived under the assumption that the skeleton grains and the pore fluid are incompressible.

e) Darcy's law

$$\mathbf{v}_w = -k \text{grad} h_w \quad (\text{A.7})$$

where  $k$  is the permeability and  $h_w$  is the total head.

f) Boundary conditions

$$\begin{aligned} \dot{\mathbf{S}}_t \mathbf{n} &= \bar{\mathbf{s}}_t \text{ on } \Gamma_t \\ \mathbf{v} &= \bar{\mathbf{v}} \text{ on } \Gamma_v \\ \bar{q} &= \bar{\mathbf{v}}_w \cdot \mathbf{n} \text{ on } \Gamma_q \\ h_w &= \bar{h}_w \text{ on } \Gamma_h \end{aligned} \quad (\text{A.8})$$

where  $\mathbf{n}$  is the unit normal vector at the boundary,  $\bar{\mathbf{s}}_t$  is the boundary value of the traction,  $\mathbf{v}$  is the velocity,  $\bar{\mathbf{v}}$  is the boundary value of the velocity,  $\bar{q}$  is the discharge per unit area with units of length per time,  $\bar{h}_w$  is the boundary head,  $\bar{\mathbf{v}}_w$  is the boundary velocity of the pore water,  $\Gamma_t$  is the stress boundary,  $\Gamma_v$  is the velocity boundary,  $\Gamma_q$  is the discharge boundary, and  $\Gamma_h$  is the hydraulic boundary.

g) Initial conditions

$$\begin{aligned} \mathbf{T}' &= \mathbf{T}'|_{t=0} \text{ in } V \\ h_w &= h_w|_{t=0} \text{ in } V \end{aligned} \quad (\text{A.9})$$

## APPENDIX B: FINITE ELEMENT FORMULATION OF GOVERNING EQUATIONS FOR SOIL–WATER COUPLED PROBLEMS

The governing equations of Equations (A.2) and (A.6) are the rate-type equilibrium equation and the conservation equation of the pore water, respectively. These equations are solved with respect to the deformation velocity and the hydraulic head with FEM. The finite element formulation under the plane strain condition for the soil–water coupled analysis in this paper is based on the procedure of Ref. [32].

The 8-node and 4-node iso-parametric quadrilateral elements are adopted for the discretization of Equation (A.2) and (A.6), respectively. The deformation velocity and the hydraulic head on an element are approximated into the following functions.

$$\mathbf{v} = [\mathbf{N}] \mathbf{v}^i, \quad h_w = [\mathbf{N}_h] h^i \quad (\text{A.10})$$

where  $[\mathbf{N}]$  and  $[\mathbf{N}_h]$  denote shape function matrices and  $\mathbf{v}^i$  and  $h^i$  are the vectors of the variables (the deformation velocity and the hydraulic head) at the nodal points surrounding the  $i$ th element. Differentiating the first equality in Equation (A.10), the deformation gradient and the stretching tensors are derived. These tensors are shrunk into vectors, as shown below, just for the matrix-based finite element formulation;

$$\{\mathbf{D}\} = (D_{11}, D_{22}, 2D_{12})^T = [\mathbf{B}] \mathbf{v}^i \quad (\text{A.11})$$

$$\{\mathbf{L}\} = (L_{11}, L_{22}, L_{12}, L_{21})^T = [\mathbf{M}] \mathbf{v}^i \quad (\text{A.12})$$

where the braces denotes the shrinkage of tensors, and  $[\mathbf{B}]$  and  $[\mathbf{M}]$  are the matrices including the derived shape functions, which produces the shrunk tensors of the deformation gradient and the stretching from the deformation velocity  $\mathbf{v}^i$  on an element. Employing the Galerkin method, the following equation is obtained by integrating the governing equations on the  $i$ th element:

$$\int_{V^i} (\text{div} \dot{\mathbf{S}}_t) \cdot \delta \mathbf{v} dV = 0 \quad (\text{A.13})$$

$$\int_{V^i} (\text{tr} \mathbf{D} + \text{div} \mathbf{v}_w) \cdot \delta h_w dV = 0 \quad (\text{A.14})$$

where  $V^i$ ,  $\delta \mathbf{v} (= [\mathbf{N}] \delta \mathbf{v}^i)$  and  $\delta h_w (= [\mathbf{N}_h] \delta h^i)$  denote the domain of the  $i$ th element, the test functions or the virtual variables for the equilibrium equation and the conservation equation of the pore water, respectively. The superscript  $i$  denotes the  $i$ th element hereafter in this appendix. The application of the divergence theorem of Gauss reduces Equations (A.13) and (A.14) into as follows:

$$\int_{\Gamma_i^i} \bar{\mathbf{s}}_t \cdot \delta \mathbf{v} ds - \int_{V^i} \dot{\mathbf{S}}_t \cdot \delta \mathbf{L} dV = 0 \quad (\text{A.15})$$

$$\int_{V^i} (\text{tr} \mathbf{D}) \delta h_w dV + \int_{\Gamma_q^i} \bar{q} \delta h_w ds - \int_{V^i} \mathbf{v}_w \cdot \text{grad} \delta h_w dV = 0 \quad (\text{A.16})$$

where  $\delta \mathbf{L}$  is defined as  $\text{grad} \delta \mathbf{v}$ . The nominal stress rate tensor  $\dot{\mathbf{S}}_t$  in Equation (A.15) is rewritten into the following form with the principle of the effective stress, which has been shown by Equation (A.3).

$$\dot{\mathbf{S}}_t = \dot{\mathbf{S}}_t' - p_w \{ (\text{tr} \mathbf{D}) \mathbf{I} - \mathbf{L}^T \} - \dot{p}_w \mathbf{I} \quad (\text{A.17})$$

where the nominal rate tensor of effective stress  $\dot{\mathbf{S}}_t'$  is defined as follows:

$$\dot{\mathbf{S}}_t' = \overset{\circ}{\mathbf{T}}' + \mathbf{T}' \text{tr} \mathbf{D} + \mathbf{W} \mathbf{T}' - \mathbf{T}' \mathbf{W} - \mathbf{T}' \mathbf{L}^T = \overset{\circ}{\mathbf{T}}' + \mathbf{T}' \text{tr} \mathbf{D} - (\mathbf{D} \mathbf{T}' + \mathbf{T}' \mathbf{D}) + \mathbf{L} \mathbf{T}' \quad (\text{A.18})$$

$$\overset{\circ}{\mathbf{T}}' = \dot{\mathbf{T}}' - \mathbf{W} \mathbf{T}' + \mathbf{T}' \mathbf{W} \quad (\text{A.19})$$

Substituting Equation (A.18) into Equation (A.15), the following equation can be obtained:

$$\int_{V^i} \overset{\circ}{\mathbf{T}}' \cdot \delta \mathbf{D} + (\text{tr} \mathbf{D}) \mathbf{T}' \cdot \delta \mathbf{D} - (\mathbf{D} \mathbf{T}' + \mathbf{T}' \mathbf{D}) \cdot \delta \mathbf{D} + \mathbf{L} \mathbf{T}' \cdot \delta \mathbf{L} - p_w (\text{tr} \mathbf{D}) \mathbf{I} \cdot \delta \mathbf{D} + p_w \mathbf{L}^T \cdot \delta \mathbf{L} - \dot{p}_w \mathbf{I} \cdot \delta \mathbf{D} dV = \int_{\Gamma_i^i} \bar{\mathbf{s}}_t \cdot \delta \mathbf{v} ds \quad (\text{A.20})$$

where  $\delta \mathbf{D}$  ( $\{\delta \mathbf{D}\} = [\mathbf{B}] \delta \mathbf{v}^i$ ) is defined as  $(\delta \mathbf{L} + \delta \mathbf{L}^T)/2$ , the symmetric part of  $\delta \mathbf{L}$  ( $\{\delta \mathbf{L}\} = [\mathbf{M}] \delta \mathbf{v}^i$ ). With the Equations (A.10)–(A.12), Equation (A.20) is reduced to the following form:

$$\left\{ \int_{V^i} [\mathbf{B}]^T [\mathbf{C}] [\mathbf{B}] + [\mathbf{B}]^T [\mathbf{T}^*] [\mathbf{B}_v] - [\mathbf{B}]^T [\mathbf{T}^{**}] [\mathbf{B}] + [\mathbf{M}]^T [\mathbf{T}^{***}] [\mathbf{M}] - [\mathbf{B}_v]^T p_w [\mathbf{B}_v] + [\mathbf{M}]^T [\mathbf{P}^*] [\mathbf{M}] dV \right\} \mathbf{v}^i - \int_{V^i} [\mathbf{B}_v]^T \dot{p}_w dV = \int_{\Gamma_i^i} [\mathbf{N}]^T \bar{\mathbf{s}}_t ds \quad (\text{A.21})$$

where  $[\mathbf{C}]$  denotes the elasto-plastic stiffness matrix derived from Equation (9), and  $[\mathbf{B}_v]$  is a matrix, which satisfies  $\text{tr} \mathbf{D} = [\mathbf{B}_v] \mathbf{v}^i$ . The detailed form of  $[\mathbf{T}^*]$ ,  $[\mathbf{T}^{**}]$ ,  $[\mathbf{T}^{***}]$ , and  $[\mathbf{P}^*]$  are listed at the end of this appendix. Letting the unit weight of water be  $\gamma_w$  and the elevation head be  $z$ ,  $\dot{p}_w$  is described as  $\gamma_w \dot{h} - \gamma_w \dot{z}$ . Therefore, Equation (A.21) can be rewritten into as follows:

$$\left\{ \int_{V^i} [\mathbf{B}]^T [\mathbf{C}] [\mathbf{B}] + [\mathbf{B}]^T [\mathbf{T}^*] [\mathbf{B}_v] - [\mathbf{B}]^T [\mathbf{T}^{**}] [\mathbf{B}] + [\mathbf{M}]^T [\mathbf{T}^{***}] [\mathbf{M}] - [\mathbf{B}_v]^T p_w [\mathbf{B}_v] + [\mathbf{M}]^T [\mathbf{P}^*] [\mathbf{M}] dV \right\} \mathbf{v}^i - \int_{V^i} [\mathbf{B}_v]^T [\mathbf{N}_h] dV (\gamma_w \mathbf{h}^i) + \int_{V^i} [\mathbf{B}_v]^T [\mathbf{G}] dV \mathbf{v}^i = \int_{\Gamma_i} [\mathbf{N}]^T \bar{\mathbf{s}}_t ds \quad (\text{A.22})$$

where  $[\mathbf{G}]$  is a matrix, which satisfies  $\gamma_w \dot{\mathbf{z}} = [\mathbf{G}] \mathbf{v}^i$

With the aid of the Darcy's law shown in Equation (A.7), Equation (A.16) is also discretized into as follows:

$$\int_{V^i} [\mathbf{N}_h]^T [\mathbf{B}_v] dV \mathbf{v}^i + \int_{\Gamma_q^i} [\mathbf{N}_h]^T \bar{q} ds + \int_{V^i} [\mathbf{B}_h]^T [\mathbf{k}] [\mathbf{B}_h] dV (\gamma_w \mathbf{h}^i) = 0 \quad (\text{A.23})$$

where  $[\mathbf{B}_h]$  is a matrix, which satisfies  $\text{grad} h_w = [\mathbf{B}_h] \mathbf{h}^i$  and  $[\mathbf{k}]$  is a two-dimensional diagonal matrix of  $\text{diag}(k/\gamma_w, k/\gamma_w)$ . Letting the increment of the nodal displacement vector be  $\Delta \mathbf{u}^i$  and the time step interval be  $\Delta t$ ,  $\mathbf{h}^i$  and  $\mathbf{v}^i$  is approximated as  $\mathbf{h}^i = (\mathbf{h}^i|_{t+\Delta t} - \mathbf{h}^i|_t) / \Delta t$  and  $\Delta \mathbf{u}^i / \Delta t$ . With these relationships, Equations (A.22) and (A.23) can be reduced to

$$[\mathbf{K}^i] \Delta \mathbf{u}^i - [\mathbf{K}_v^i]^T (\gamma_w \mathbf{h}^i|_{t+\Delta t}) = \Delta \mathbf{F}^i - [\mathbf{K}_v^i]^T (\gamma_w \mathbf{h}^i|_t) \quad (\text{A.24a})$$

$$-[\mathbf{K}_v^i] \Delta \mathbf{u}^i - (1 - \theta) \Delta t [\mathbf{K}_h^i] (\gamma_w \mathbf{h}^i|_{t+\Delta t}) = \Delta \mathbf{Q}^i + \theta \Delta t [\mathbf{K}_h^i] (\gamma_w \mathbf{h}^i|_t) \quad (\text{A.24b})$$

$$[\mathbf{K}^i] = \int_{V^i} [\mathbf{B}]^T [\mathbf{C}] [\mathbf{B}] + [\mathbf{B}]^T [\mathbf{T}^*] [\mathbf{B}_v] - [\mathbf{B}]^T [\mathbf{T}^{**}] [\mathbf{B}] + [\mathbf{M}]^T [\mathbf{T}^{***}] [\mathbf{M}] - [\mathbf{B}_v]^T p_w [\mathbf{B}_v] + [\mathbf{M}]^T [\mathbf{P}^*] [\mathbf{M}] + [\mathbf{B}_v]^T [\mathbf{G}] dV, [\mathbf{K}_v^i] = \int_{V^i} [\mathbf{N}_h]^T [\mathbf{B}_v] dV, [\mathbf{K}_h^i] = \int_{V^i} [\mathbf{B}_h]^T [\mathbf{k}] [\mathbf{B}_h] dV \quad (\text{A.24c})$$

where  $\theta$  ( $0 \leq \theta \leq 1$ ) is the time-varying coefficient. In assembling Equation (A.24) for each element into a global system of equations for all nodal variables, the matrix form of the global equations is obtained as follows;

$$\begin{bmatrix} [\mathbf{K}] & -[\mathbf{K}_v]^T \\ -[\mathbf{K}_v] & -\Delta t (1 - \theta) [\mathbf{K}_h] \end{bmatrix} \begin{Bmatrix} \Delta \mathbf{u} \\ \gamma_w \mathbf{h}|_{t+\Delta t} \end{Bmatrix} = \begin{Bmatrix} \Delta \mathbf{F} - [\mathbf{K}_v]^T \gamma_w \mathbf{h}|_t \\ \Delta \mathbf{Q} + \Delta t \theta [\mathbf{K}_h] \gamma_w \mathbf{h}|_t \end{Bmatrix} \quad (\text{A.25})$$

where  $[\mathbf{K}]$ ,  $[\mathbf{K}_v]$ ,  $[\mathbf{K}_h]$ ,  $\Delta \mathbf{u}$ ,  $\mathbf{h}$ ,  $\Delta \mathbf{F}$  and  $\Delta \mathbf{Q}$  are assembled global matrices or vectors from  $[\mathbf{K}^i]$ ,  $[\mathbf{K}_v^i]$ ,  $[\mathbf{K}_h^i]$ ,  $\Delta \mathbf{u}^i$ ,  $\mathbf{h}^i$ ,  $\Delta \mathbf{F}^i$  and  $\Delta \mathbf{Q}^i$ , respectively.

$$[\mathbf{T}^*] = \begin{bmatrix} T'_{11} \\ T'_{22} \\ T'_{12} \end{bmatrix}, [\mathbf{T}^{**}] = \begin{bmatrix} 2T'_{11} & 0 & T'_{12} \\ 0 & 2T'_{22} & T'_{12} \\ T'_{12} & T'_{12} & (T'_{11} + T'_{22})/2 \end{bmatrix}, [\mathbf{T}^{***}] = \begin{bmatrix} T'_{11} & 0 & T'_{12} & 0 \\ 0 & T'_{22} & 0 & T'_{12} \\ T'_{12} & 0 & T'_{22} & 0 \\ 0 & T'_{12} & 0 & T'_{11} \end{bmatrix} \quad (\text{A.26})$$

$$[\mathbf{P}^*] = \begin{bmatrix} p_w & 0 & 0 & 0 \\ 0 & p_w & 0 & 0 \\ 0 & 0 & 0 & p_w \\ 0 & 0 & p_w & 0 \end{bmatrix} \quad (\text{A.27})$$

#### ACKNOWLEDGEMENTS

This work has been supported by the Grant-in-Aid for Scientific Research (B), # 20380136, of the Japanese Society for Promotion of Science (JSPS). This support is gratefully acknowledged.

## REFERENCES

1. Bui HD. *Inverse problems in the mechanics of materials, An introduction*. CRC Press: USA, 1993.
2. Tarantola A. *Inverse problem theory*. Elsevier: England, 1987.
3. Calvello M, Finno RJ. Selecting parameters to optimize in model calibration by inverse analysis. *Computers and Geotechnics* 2004; **31**:411–425.
4. Gioda G, Sakurai S. Back analysis procedures for the interpretation of field measurements in geomechanics. *International Journal for Numerical and Analytical Methods in Geomechanics* 1987; **11**(6):555–583.
5. Lecampion B, Constantinescu A. Sensitivity analysis for parameter identification in quasi-static poroplasticity. *International Journal for Numerical and Analytical Methods in Geomechanics* 2005; **29**:163–185.
6. Ledesma A, Gens A, Alonso EE. Estimation of parameters in geotechnical backanalysis — I. Maximum likelihood approach. *Computers and Geotechnics* 1996; **18**(1):1–27.
7. Ledesma A, Gens A, Alonso EE. Estimation of parameters in geotechnical backanalysis — II. Application to a tunnel excavation problem. *Computers and Geotechnics* 1996; **18**(1):29–46.
8. Ledesma A, Gens A, Alonso EE. Parameter and variance estimation in geotechnical backanalysis using prior information. *International Journal for Numerical and Analytical Methods in Geomechanics* 1996; **20**:119–141.
9. Hashash YMA, Levasseur S, Osouli A, Finno R, Malecot Y. Comparison of two inverse analysis techniques for learning deep excavation systems. *Computers and Geotechnics* 2009; **37**(3):323–333.
10. Levasseur S, Malecot Y, Boulon M, Flavigny E. Statistical inverse analysis based on genetic algorithm and principal component analysis: Method and developments using synthetic data. *International Journal for Numerical and Analytical Methods in Geomechanics* 2009; **33**:1485–1511.
11. Levasseur S, Malecot Y, Boulon M, Flavigny E. Statistical inverse analysis based on genetic algorithm and principal component analysis: Applications to excavation problems and pressuremeter tests. *International Journal for Numerical and Analytical Methods in Geomechanics* 2010; **34**:471–491.
12. Reccha C, Levasseur S, Finno R. Inverse analysis techniques for parameter identification in simulation of excavation support systems. *Computers and Geotechnics* 2008; **35**:331–345.
13. Nakamura T, Gu Y. Identification of elastic–plastic anisotropic parameters using instrumented indentation and inverse analysis. *Mechanics of Materials* 2007; **39**:340–356.
14. Murakami A. The role of Kalman filtering in an inverse analysis of elasto-plastic material. *Proceedings of the Japan Academy Series B* 2002; **78**(8):250–255.
15. Courtier P, Thepaut T, Hollingsworth A. A strategy for operational implementation of 4DVAR using an incremental approach. *Quarterly Journal of the Royal Meteorological Society* 1994; **120**(519):1367–1387.
16. Evensen G. Sequential data assimilation with a non-linear quasi-geostrophic model using Monte Carlo methods to forecast error statistics. *Journal of Geophysical Research* 1994; **99**:10143–10621.
17. Evensen G. *Data assimilation: The ensemble Kalman filter*. Springer: Berlin, 2006.
18. Gordon NJ, Salmond DJ, Smith AFM. Novel approach to nonlinear/non-Gaussian Bayesian state estimation. *IEE Proceedings-F* 1993; **140**(2):107–113.
19. Kitagawa G. Monte Carlo filter and smoother for non-Gaussian nonlinear state space mode. *Journal of Computational and Graphical Statistics* 1996; **5**(1):1–25.
20. Kalman RE. A new approach to linear filtering and prediction problems. *Journal of Basic Engineering* 1960; **82**:35–45.
21. Murakami A, Hasegawa T. Back analysis by Kalman filter finite elements and optimal location of observed points. In *Numerical Methods in Geomechanics*, Swoboda G (ed.). Balkema: Rotterdam, 1988; 2051–2058.
22. Murakami A. Application of Kalman filtering to some geomechanical problems related to safety assessment. *Doctoral Dissertation*, Kyoto University, 1991.
23. Bittanti S, Maier G, Nappi A. Inverse problems in structural elasto-plasticity: a Kalman filter approach. In *Plasticity Today*, Sawczuk A, Bianchi G (eds). Elsevier Applied Science Publishers: London, 1984; 311–329.
24. Fedele R, Maier G, Whelan M. Stochastic calibration of local constitutive models through measurements at the macroscale in heterogeneous media. *Computer Methods in Applied Mechanics and Engineering* 2006; **195**:4971–4990.
25. Chen Y, Zhang D. Data assimilation for transient flow in geologic formations via ensemble Kalman filter. *Advances in Water Resources* 2006; **29**:1107–1122.
26. Hommels A, Murakami A, Nishimura S. A comparison of the ensemble Kalman filter with the unscented Kalman filter: application to the construction of a road embankment. *GEO International* 2009:52–54.
27. Chatzi EN, Smyth AW. The unscented Kalman filter and particle filter methods for nonlinear structural system identification with non-collocated heterogeneous sensing. *Structural Control and Health Monitoring* 2009; **16**:99–123.
28. Namdeo V, Manohar CS. Nonlinear structural dynamical system identification using adaptive particle filters. *Journal of Sound and Vibration* 2007; **306**:524–563.
29. Sajeeb R, Monahar CS, Roy D. A conditionally linearized Monte Carlo filter in non-linear structural dynamics. *International Journal of Non-linear Mechanics* 2009; **44**:776–790.
30. Sajeeb R, Monahar CS, Roy D. A semi-analytical particle filter for identification of nonlinear oscillators. *Probabilistic Engineering Mechanics* 2010; **25**:35–48.
31. Asaoka A, Nakano M, Noda T. Soil-water coupled behavior of heavily overconsolidated clay near/at critical state. *Soils and Foundations* 1997; **37**(1):13–28.
32. Yatomi C, Yashima A, Iizuka A, Sano I. Shear bands formation numerically simulated by a non-coaxial cam-clay model. *Soils and Foundations* 1989; **29**(4):1–13.

33. Nakamura K, Higuchi T, Hirose N. Sequential data assimilation: Information fusion of a numerical simulation and large scale observation data. *Journal of Universal Computer Science* 2006; **12**(6):608–626.
34. Nakano S, Ueno G, Higuchi T. Merging particle filter for sequential data assimilation. *Nonlinear Processes in Geophysics* 2007; **14**:395–408.
35. Doucet A, Godsill S, Andrieu C. On sequential Monte Carlo sampling methods for Bayesian filtering. *Statistics and Computing* 2000; **10**:197–208.
36. Ghosh SJ, Manohar CS, Roy D. A sequential importance sampling filter with a new proposal distribution for state and parameter identification of nonlinear dynamical systems. *Proceedings of the Royal Society Series A* 2008; **464**:25–47.
37. Shuku T, Murakami A, Nishimura S, Fujisawa K, Nakamura K. Data assimilation of the settlement behavior of Kobe Airport constructed on reclaimed land using the particle filter. *Journal of Applied Mechanics* 2010; **13**:67–77 (in Japanese).
38. Yamamoto T, Sakagami T, Takahashi Y, Yagiura Y, Nambu M, Iizuka A. Establishment of soil deformation analysis method at Kobe Airport. *Proceedings of JSCE C* 2010; **66**(3):457–451 (in Japanese).
39. Hasaegawa N, Yagiura Y, Takahashi Y, Wada M, Iizuka A. Behavior of alluvial cohesive soils in Kobe Airport construction project. *Japanese Geotechnical Journal* 2007; **2**(1):25–35 (in Japanese).
40. Asaoka A, Nakano M, Fernando GSK, Nozu M. Mass permeability concept in the analysis of treated ground with sand drains. *Soils and Foundations* 1995; **35**(3):43–53.